Revised Version

JHEP 0611 (2006) 048
DESY 06-108
ZH-TH 17/06

DESY 06-108
ZH–TH 17/06

Electroweak two-loop corrections to the effective weak mixing angle

M. Awramik[1*], M. Czakon[2†] and A. Freitas[3‡]

[1] *II. Institut für Theoretische Physik, Universität Hamburg, Luruper Chaussee 149, D-22761 Hamburg, Germany*
and
Institute of Nuclear Physics, Radzikowskiego 152, PL-31342 Kraków, Poland

[2] *Institut für Theoretische Physik und Astrophysik, Universität Würzburg, Am Hubland, D-97074 Würzburg, Germany*
and
Institute of Physics, University of Silesia, Uniwersytecka 4, PL-40007 Katowice, Poland

[3] *Institut für Theoretische Physik, Universität Zürich, Winterthurerstrasse 190, CH-8057 Zürich, Switzerland*

Abstract

Recently exact results for the complete electroweak two-loop contributions to the effective weak mixing angle were published. This paper illustrates the techniques used for this computation, in particular the methods for evaluating the loop diagrams and the proper definition of Z-pole observables at next-to-next-to-leading order. Numerical results are presented in terms of simple parametrization formulae and compared in detail with a previous result of an expansion up to next-to-leading order in the top-quark mass. Finally, an estimate of the remaining theoretical uncertainties from unknown higher-order corrections is given.

*email: Malgorzata.Awramik@desy.de
†email: mczakon@yahoo.com
‡email: afreitas@physik.unizh.ch

1 Introduction

One of the most important quantities for testing the Standard Model or its extensions is the sine of the effective leptonic weak mixing angle $\sin^2\theta_{\rm eff}^{\rm lept}$. In the global fit of the Standard Model to all relevant electroweak data, the effective leptonic weak mixing angle has a strong impact on indirect constraints on $M_{\rm H}$. It can be defined through the effective vector and axial-vector couplings, v_l and a_l, of the Z boson to leptons (l) at the Z boson pole. Writing the Z boson-lepton vertex as $\Gamma[Zl^+l^-] = i\,\bar{l}\gamma^\mu(v_l + a_l\gamma_5)l\;Z_\mu$, one obtains

$$\sin^2\theta_{\rm eff}^{\rm lept} = \frac{1}{4}\left(1 + {\rm Re}\,\frac{v_l}{a_l}\right). \tag{1}$$

Experimentally, $\sin^2\theta_{\rm eff}^{\rm lept}$ is derived from various asymmetries measured around the Z boson peak at e^+e^- colliders after subtraction of QED effects. It can also be determined from asymmetries measured at center-of-mass energies away from the Z pole, requiring a theoretical extrapolation in order to match it to $\sin^2\theta_{\rm eff}^{\rm lept}$ on the Z pole. The current experimental accuracy, $\sin^2\theta_{\rm eff}^{\rm lept} = 0.23147 \pm 0.00017$ [1], could be improved by an order of magnitude at a future high-luminosity linear collider running in a low-energy mode at the Z boson pole (Giga$Z$) [2]. This offers the prospect for highly sensitive tests of the electroweak theory [3], provided that the accuracy of the theoretical prediction matches the experimental precision.

Typically, the theoretical prediction of $\sin^2\theta_{\rm eff}^{\rm lept}$ within the Standard Model is given in terms of the following input parameters: the fine structure constant α, the Fermi constant G_μ, the Z-boson mass $M_{\rm Z}$ and the top-quark mass $m_{\rm t}$ (and other fermion masses whenever they are numerically relevant). The W-boson mass $M_{\rm W}$ is calculated from the Fermi constant, which is precisely derived from the muon decay lifetime. As a consequence, the computation of $\sin^2\theta_{\rm eff}^{\rm lept}$ involves two major parts: the radiative corrections to the relation between G_μ and $M_{\rm W}$, and the corrections to the Z-lepton vertex form factors. The latter can be incorporated into the quantity $\kappa = 1 + \Delta\kappa$, defined in the on-shell scheme,

$$\sin^2\theta_{\rm eff}^{\rm lept} = \left(1 - M_{\rm W}^2/M_{\rm Z}^2\right)(1 + \Delta\kappa), \tag{2}$$

At tree-level, $\Delta\kappa = 0$ and the sine of the effective mixing angle is identical to the sine of the on-shell weak mixing angle $\sin^2\theta_{\rm W} \equiv s_{\rm W} = 1 - M_{\rm W}^2/M_{\rm Z}^2$. The quantity $\Delta\kappa$ is only weakly sensitive to $M_{\rm W}$.

For the computation of the W-boson mass, the complete electroweak two-loop corrections, including partial higher-order corrections, have been carried out in Ref. [4–7]. In this report, the calculation of the corresponding contributions for the form factor $\Delta\kappa$ and combined predictions for $\sin^2\theta_{\rm eff}^{\rm lept}$ will be discussed.

The quantum corrections to $\sin^2\theta_{\rm eff}^{\rm lept}$ have been under extensive theoretical study over the last two decades. The one-loop result [8, 9] involves large fermionic contributions from the leading contribution to the ρ parameter, $\Delta\rho$, which is quadratically dependent on the top-quark mass $m_{\rm t}$, resulting from the top-bottom mass splitting [10]. The correction $\Delta\rho$

enters both in the computation of $M_{\rm W}$ from the Fermi constant (for a discussion see e.g. Ref. [4, 5]), as well as into the vertex correction factor $\Delta\kappa$,

$$1 + \Delta\kappa^{(\alpha)} = 1 + \frac{c_{\rm W}^2}{s_{\rm W}^2}\Delta\rho + \Delta\kappa_{\rm rem}(M_{\rm H}), \tag{3}$$

with $c_{\rm W}^2 = M_{\rm W}^2/M_{\rm Z}^2$, $s_{\rm W}^2 = 1 - M_{\rm W}^2/M_{\rm Z}^2$. The remainder part $\Delta\kappa_{\rm rem}$ contains in particular the dependence on the Higgs-boson mass, $M_{\rm H}$.

Beyond the one-loop order, resummations of the leading one-loop contribution $\Delta\rho$ have been derived [11, 12]. They correctly take into account the terms of the form $(\Delta\rho)^2$ and $(\Delta\alpha\Delta\rho)$. Here $\Delta\alpha$ is the shift in the fine structure constant due to light fermions, $\Delta\alpha \propto \log m_f$, which enters through the corrections to the relation between G_μ and $M_{\rm W}$, since $\Delta\kappa = \Delta\kappa(M_{\rm W})$ is a function of $M_{\rm W}$. These resummation results have been confirmed and extended by an explicit calculation of the pure fermion-loop corrections at $\mathcal{O}(\alpha^2)$ (i.e. contributions containing two fermion loops) [13]. Recently, the leading three-loop contributions to the ρ parameter of $\mathcal{O}(G_\mu^3 m_{\rm t}^6)$ and $\mathcal{O}(G_\mu^2\alpha_{\rm s} m_{\rm t}^4)$ for large top-quark mass [14], as well as $\mathcal{O}(G_\mu^3 M_{\rm H}^4)$ for large Higgs mass [15] have been computed.

Higher order QCD corrections to $\sin^2\theta_{\rm eff}^{\rm lept}$ have been calculated at $\mathcal{O}(\alpha\alpha_{\rm s})$ [16] and for the top-bottom contributions at $\mathcal{O}(\alpha\alpha_{\rm s}^2)$ [17] and $\mathcal{O}(\alpha\alpha_{\rm s}^3)$ [18]. The $\mathcal{O}(\alpha\alpha_{\rm s}^2)$ contributions with light quarks in the loops can be derived from eqs. (29)–(31) in [19] and turn out to be completely negligible. For the electroweak two-loop contributions, only partial results using large mass expansions in the Higgs mass [20] and top-quark mass [21–23] have been known previously. Concerning the expansion in $m_{\rm t}$, the formally leading term of $\mathcal{O}(G_\mu^2 m_{\rm t}^4)$ [21, 22] and the next-to-leading term of $\mathcal{O}(G_\mu^2 m_{\rm t}^2 M_{\rm Z}^2)$ [23] were found to be numerically significant and of similar magnitude. Therefore, a complete calculation of electroweak two-loop corrections to $\sin^2\theta_{\rm eff}^{\rm lept}$ beyond the leading terms of expansions is desirable.

As a first step in this direction, exact results have been obtained for the Higgs-mass dependence (i.e. the quantity $\sin^2\theta_{\rm eff,sub}^{\rm lept}(M_{\rm H}) \equiv \sin^2\theta_{\rm eff}^{\rm lept}(M_{\rm H}) - \sin^2\theta_{\rm eff}^{\rm lept}(M_{\rm H} = 65\ {\rm GeV})$) of the two-loop corrections with at least one closed fermion loop to the precision observables [13,24]. They were shown to agree well with the previous results of the top-quark mass expansion [25].

This paper discusses the complete computation of all electroweak two-loop corrections to $\sin^2\theta_{\rm eff}^{\rm lept}$. In addition to the corrections to the prediction of the W-boson mass, which have been analyzed before [4, 5], this includes all two-loop diagrams contributing to the Zl^+l^- vertex on the Z pole. The diagrams can be conveniently divided into two groups; *fermionic* contributions with at least one closed fermion loop, and *bosonic* contributions without closed fermion loops. The genuine fermionic two-loop vertex diagrams are represented by the generic topologies in Fig. 1 and some examples of bosonic two-loop diagrams are given in Fig. 2.

Results for the complete two-loop corrections have been presented first in Ref. [26, 27]. The results for the fermionic contributions have been confirmed in Ref. [28] and partial results for the bosonic contributions were also obtained in Ref. [29]. This paper describes the computational methods and analysis in more detail.

The paper is organized as follows. In section 2, the process $e^+e^- \to l^+l^-$ is analyzed at

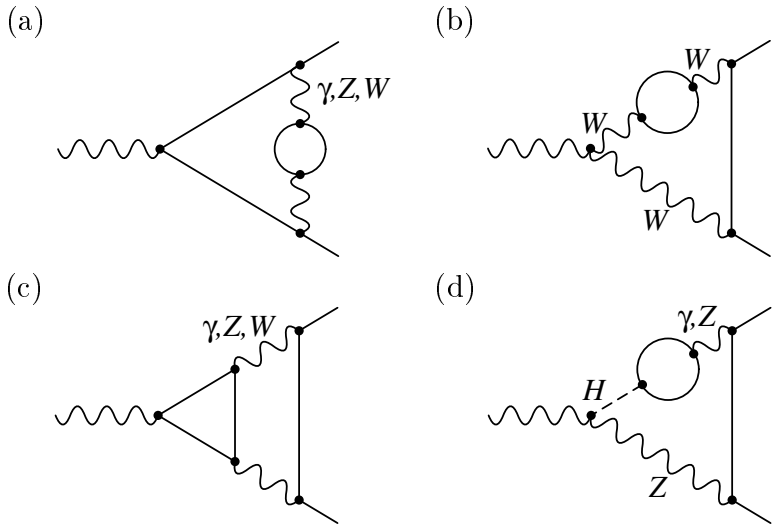

Figure 1: Genuine fermionic two-loop Zl^+l^- vertex diagrams contributing to $\sin^2\theta^{\rm lept}_{\rm eff}$.

next-to-next-to-leading order near the Z-boson pole and the $\mathcal{O}(\alpha^2)$ definition of the $\sin^2\theta^{\rm lept}_{\rm eff}$ is extracted. Furthermore the general strategies for the calculation of two-loop contributions to the form factor $\Delta\kappa$ are discussed. Sections 3 and 4 explain the calculation of the fermionic and bosonic two-loop diagrams in detail. For two-loop vacuum and self-energy diagrams, well-established techniques exist and have been used for the computation of $M_{\rm W}$ [4–6]. The new part in this project are the two-loop vertex topologies, which have been treated with two conceptually independent methods. A discussion of the numerical results and remaining theoretical uncertainties due to unknown higher orders can be found in section 5. In addition to the effective leptonic weak mixing angle, results are given also for the effective weak mixing angle for other final state flavors, i.e. for couplings of the Z boson to other fermions. Finally the implementation of our new results into the program ZFITTER is described.

2 Outline of the calculation

The two-loop corrections to the effective weak mixing angle $\sin^2\theta^f_{\rm eff}$ are part of the next-to-next-to-leading order corrections to the process $e^+e^- \to f\bar{f}$ for center-of-mass energies near the Z-boson mass, $\sqrt{s} \approx M_{\rm Z}$. To set the scene for this calculation, a framework for the next-to-next-to-leading order analysis of $f\bar{f}$ production needs to be established. Furthermore it has to be checked whether $\sin^2\theta^f_{\rm eff}$ is a well-defined, i.e. gauge-invariant and finite, quantity at this order in perturbation theory.

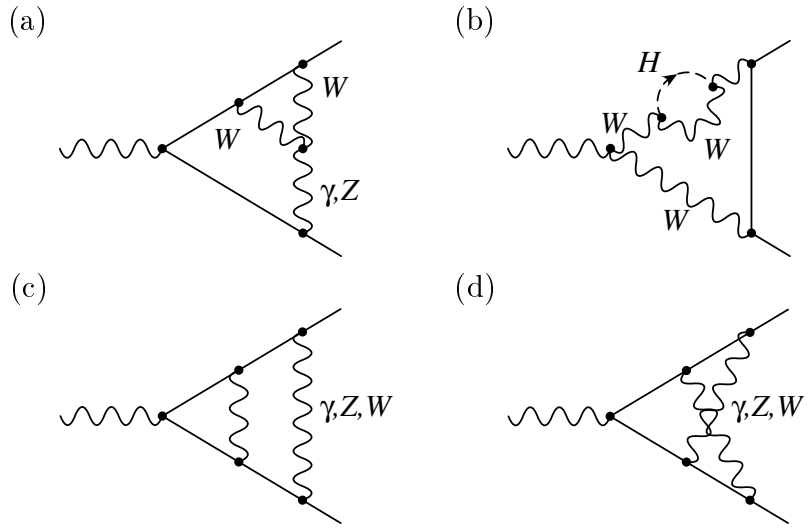

Figure 2: Examples of bosonic two-loop Zl^+l^- vertex diagrams contributing to $\sin^2\theta_{\rm eff}^{\rm lept}$.

2.1 Definition of the effective weak mixing angle at next-to-next-to-leading order

In higher-order calculations, occurrences of unstable intermediate particles need to be treated carefully in order to preserve gauge-invariance and unitarity. Currently, the only scheme proven to fulfill both requirements to all orders in perturbation theory is the *pole scheme* [30–32]. It involves a systematic Laurent expansion around the complex pole $\mathcal{M}^2 = M^2 - iM\Gamma$ associated with the propagator of the unstable particle with mass M and width Γ. In the case of the process $e^+e^- \to f\bar{f}$, $e \neq f$, near the Z pole, the amplitude is written as

$$\mathcal{A}[e^+e^- \to f\bar{f}] = \frac{R}{s - \mathcal{M}_{\rm Z}^2} + S + (s - \mathcal{M}_{\rm Z}^2)S' + \dots \tag{4}$$

with

$$\mathcal{M}_{\rm Z}^2 = \overline{M}_{\rm Z}^2 - i\overline{M}_{\rm Z}\overline{\Gamma}_{\rm Z}. \tag{5}$$

Owing to the analyticity of the S-matrix, all coefficients of Laurent expansion, $R, S, S', \dots$ and the pole location $\mathcal{M}_{\rm Z}^2$ are individually gauge-invariant, UV- and IR-finite, when soft and collinear real photon emission is added.

The first term in (4) corresponds to a Breit-Wigner parametrization of the Z line shape with a constant decay width. Experimentally, however, the gauge-boson mass is determined based on a Breit-Wigner function with a running (energy-dependent) width,

$$\mathcal{A} \propto \frac{1}{s - M_{\rm Z}^2 + is\Gamma_{\rm Z}/M_{\rm Z}}. \tag{6}$$

As a consequence of these different parameterizations, there is a shift between the experimental mass parameter, $M_{\rm Z}$, and the mass parameter of the pole scheme, $\overline{M}_{\rm Z}$, [33],

$$\overline{M}_{\rm Z}^2 = M_{\rm Z}^2/(1 + \Gamma_{\rm Z}^2/M_{\rm Z}^2), \tag{7}$$

amounting to $\overline{M}_{\rm Z} \approx M_{\rm Z} - 34.1$ MeV. In the following, barred quantities always refer to pole scheme parameters.

The evaluation of higher order contributions in the pole scheme involves a simultaneous expansion around the pole location and in the perturbation order α. Since near the Z pole α, $\Gamma_{\rm Z}$ and $(s - \mathcal{M}_{\rm Z}^2)$ are all of the same order, for a next-to-next-leading order calculation R needs to be determined to $\mathcal{O}(\alpha^2)$, S only to $\mathcal{O}(\alpha)$, while a tree-level result is sufficient for S'.

The effective weak mixing angle is contained in the pole term residue R in (4). For further use, the following notations for vertex and self-energy form factors are introduced,

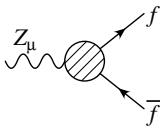

$$\equiv \Gamma[Z_\mu f \bar{f}] \equiv z_{{\rm f},\mu} = i\gamma_\mu (v_{\rm f} + a_{\rm f}\gamma_5), \tag{8}$$

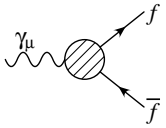

$$\equiv \Gamma[\gamma_\mu f \bar{f}] \equiv g_{{\rm f},\mu} = i\gamma_\mu (q_{\rm f} + p_{\rm f}\gamma_5), \tag{9}$$

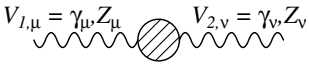

$$= \Sigma^{\mu\nu}_{V_1 V_2}, \tag{10}$$

where the shaded blobs stand for one-particle irreducible loop contributions. It is also convenient to define $Zf\bar{f}$ vertex form factors including the effect of Z-γ mixing,

$$\begin{aligned}
\hat{z}_{{\rm f},\mu}(k^2) &= i\gamma_\mu \left[\hat{v}_{\rm f}(k^2) + \hat{a}_{\rm f}(k^2)\gamma_5\right] \\
&\equiv i\gamma_\mu \left[v_{\rm f}(k^2) + a_{\rm f}(k^2)\gamma_5\right] - i\gamma_\mu \left[q_{\rm f}(k^2) + p_{\rm f}(k^2)\gamma_5\right] \frac{\Sigma_{\gamma Z}(k^2)}{k^2 + \Sigma_{\gamma\gamma}(k^2)} \\
&= \quad + \quad + \quad + \ldots ,
\end{aligned} \tag{11}$$

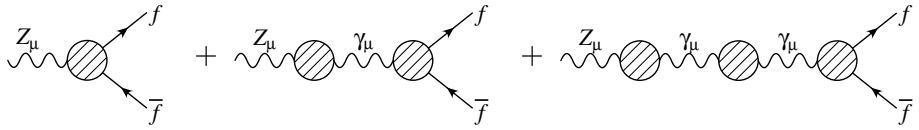

where k is the momentum of the external Z line. With these definitions, the residue R up to next-to-next-to-leading order can be cast into the form [31]

$$\begin{aligned}
R = {} & z_{\rm e}^{(0)}\, R_{ZZ}\, z_{\rm f}^{(0)} + \left[\hat{z}_{\rm e}^{(1)}(M_{\rm Z}^2)\, z_{\rm f}^{(0)} + z_{\rm e}^{(0)}\, \hat{z}_{\rm f}^{(1)}(M_{\rm Z}^2)\right] \left[1 + \Sigma_{\gamma Z}^{(1)\prime}(M_{\rm Z}^2)\right] \\
& + \hat{z}_{\rm e}^{(2)}(M_{\rm Z}^2)\, z_{\rm f}^{(0)} + z_{\rm e}^{(0)}\, \hat{z}_{\rm f}^{(2)}(M_{\rm Z}^2) + \hat{z}_{\rm e}^{(1)}(M_{\rm Z}^2)\, \hat{z}_{\rm f}^{(1)}(M_{\rm Z}^2) \\
& - iM_{\rm Z}\Gamma_{\rm Z} \left[\hat{z}_{\rm e}^{(1)\prime}(M_{\rm Z}^2)\, z_{\rm f}^{(0)} + z_{\rm e}^{(0)}\, \hat{z}_{\rm f}^{(1)\prime}(M_{\rm Z}^2)\right],
\end{aligned} \tag{12}$$

$$\begin{aligned}
R_{ZZ} = {} & 1 - \Sigma_{ZZ}^{(1)\prime}(M_{\rm Z}^2) \\
& - \Sigma_{ZZ}^{(2)\prime}(M_{\rm Z}^2) + \left(\Sigma_{ZZ}^{(1)\prime}(M_{\rm Z}^2)\right)^2 + iM_{\rm Z}\Gamma_{\rm Z}\, \Sigma_{ZZ}^{(1)\prime\prime}(M_{\rm Z}^2) \\
& - \frac{1}{M_{\rm Z}^4} \left(\Sigma_{\gamma Z}^{(1)}(M_{\rm Z}^2)\right)^2 + \frac{2}{M_{\rm Z}^2}\, \Sigma_{\gamma Z}^{(1)}(M_{\rm Z}^2)\, \Sigma_{\gamma Z}^{(1)\prime}(M_{\rm Z}^2).
\end{aligned} \tag{13}$$

Here the Lorentz indices have been suppressed. Based on the definition of $\sin^2\theta^{\rm lept}_{\rm eff}$ in eqs. (1),(2), the two-loop result of the effective weak mixing angle is derived from R as

$$\begin{aligned}\sin^2\theta^f_{\rm eff} &\equiv \left(1-\frac{\overline{M}^2_{\rm W}}{\overline{M}^2_{\rm Z}}\right)\mathrm{Re}\left\{1+\Delta\overline{\kappa}^{\rm f}_{\rm Z}(M^2_{\rm Z})\right\}\\ &= \left(1-\frac{\overline{M}^2_{\rm W}}{\overline{M}^2_{\rm Z}}\right)\mathrm{Re}\left\{1+\left.\frac{\hat{a}^{(1)}_{\rm f}\,v^{(0)}_{\rm f}-\hat{v}^{(1)}_{\rm f}\,a^{(0)}_{\rm f}}{a^{(0)}_{\rm f}(a^{(0)}_{\rm f}-v^{(0)}_{\rm f})}\right|_{k^2=M^2_{\rm Z}}\right.\\ &\qquad\left.+\left.\frac{\hat{a}^{(2)}_{\rm f}\,v^{(0)}_{\rm f}\,a^{(0)}_{\rm f}-\hat{v}^{(2)}_{\rm f}\,(a^{(0)}_{\rm f})^2-(\hat{a}^{(1)}_{\rm f})^2\,v^{(0)}_{\rm f}+\hat{a}^{(1)}_{\rm f}\,\hat{v}^{(1)}_{\rm f}\,a^{(0)}_{\rm f}}{(a^{(0)}_{\rm f})^2(a^{(0)}_{\rm f}-v^{(0)}_{\rm f})}\right|_{k^2=M^2_{\rm Z}}\right\}.\end{aligned} \tag{14}$$

Since the pole scheme is based on a formal Laurent series of the physical amplitude, all coefficients in the expansion and thus the effective weak mixing angle are manifestly gauge-invariant and UV-finite. While the pole scheme formalism does not make any statement about IR finiteness, it can be checked that eq. (14) is also a IR-safe quantity, i.e. all IR-divergencies from photon exchange diagrams cancel. Similarly, collinear divergencies (or Sudakov factors for massive fermions) also cancel. This can be explained by the fact that the QED contributions in the soft and collinear limits factorize from massive loop effects and therefore drop out in the ratio of the vector and axial-vector form factor in eq. (1). At the diagrammatic level, this cancellation of divergencies occurs not only between two-loop diagrams, but also between 2-loop and products of 1-loop diagrams, for example

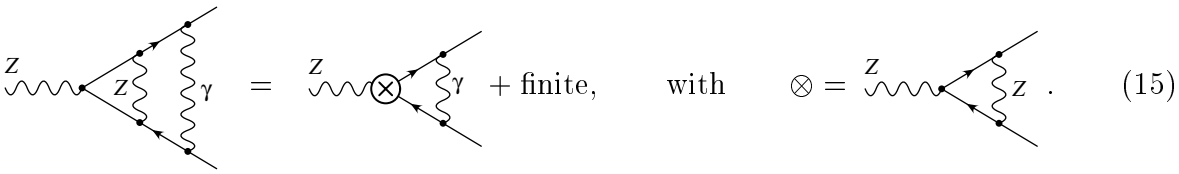

(15)

Experimentally, the effective weak mixing angle is determined from measurements of forward-backward and left-right asymmetries of the process $e^+e^-\to f\bar{f}$. The derivation of $\sin^2\theta^f_{\rm eff}$ from these asymmetries requires the subtraction of effects from QED and QCD corrections, s-channel photon exchange and γ-Z interference, off-shellness of the Z-boson and box contributions. These non-resonant effects enter into the amplitude through the next-to-leading term S in the pole expansion (4), and need to be computed up to one-loop order. In order to relate the $\mathcal{O}(\alpha^2)$ result (14) for $\sin^2\theta^f_{\rm eff}$ to the value quoted by the experimental analyses, it needs to be checked that the subtracted effects are consistent with the pole scheme prescription.

In experimental studies, the program ZFITTER [35] is widely used for prediction of the contributions from QED and QCD corrections, s-channel photon exchange and γ-Z interference, off-shellness of the Z-boson and box contributions. In ZFITTER, the radiative correc-

tions to the process $e^+e^- \to f\bar{f}$ are parametrized by four form factors $\rho_{\rm ef}$, $\kappa_{\rm e}$, $\kappa_{\rm f}$, $\kappa_{\rm ef}$,

$$\begin{aligned}
\mathcal{A}[e^+e^- \to f\bar{f}] = 4\pi i\,\alpha\,\frac{Q_{\rm e}Q_{\rm f}}{s}\,\gamma_\mu \otimes \gamma^\mu \\
+ i\frac{\sqrt{2}G_\mu M_{\rm Z}^2}{1+i\Gamma_{\rm Z}/M_{\rm Z}}\,I_{\rm e}^{(3)}\,I_{\rm f}^{(3)}\,\frac{1}{s-\overline{M}_{\rm Z}^2+i\overline{M}_{\rm Z}\overline{\Gamma}_{\rm Z}} \\
\times \rho_{\rm ef}\,\Big[\gamma_\mu(1+\gamma_5)\otimes\gamma^\mu(1+\gamma_5) \\
- 4|Q_{\rm e}|s_{\rm W}^2\,\kappa_{\rm e}\,\gamma_\mu\otimes\gamma^\mu(1+\gamma_5) \\
- 4|Q_{\rm f}|s_{\rm W}^2\,\kappa_{\rm f}\,\gamma_\mu(1+\gamma_5)\otimes\gamma^\mu \\
+ 16|Q_{\rm e}Q_{\rm f}|s_{\rm W}^4\,\kappa_{\rm ef}\,\gamma_\mu\otimes\gamma^\mu\Big]
\end{aligned} \tag{16}$$

Note that apart from the Z propagator, the gauge boson masses are defined according to the running width prescription (un-barred symbols) instead of the pole scheme definition (barred symbols). As a result the form factors $\kappa_{\rm e}$, $\kappa_{\rm f}$, $\kappa_{\rm ef}$ can differ from the corresponding form factors $\overline{\kappa_{\rm e}}$, $\overline{\kappa_{\rm f}}$, $\overline{\kappa_{\rm ef}}$ in the pole scheme. In the following, the relation between the two sets of quantities will be worked out.

ZFITTER includes all radiative corrections to $e^+e^- \to f\bar{f}$ consistently at the one-loop level with some leading two-loop contributions. However, it has not been designed for a complete next-to-next-to-leading order analysis and inconsistencies could occur at this level. In ZFITTER QED and QCD corrections are included via a convolution of the cross-section. They will be discussed in more detail later. The effects from s-channel photon exchange, γ-Z interference, off-shellness of the Z-boson and massive (non-QED) box contributions are taken into account by the formulae [35]

$$\begin{aligned}
\kappa_{\rm ef}(s) = \kappa_{\rm e}(s)\kappa_{\rm f}(s) - \frac{M_{\rm Z}^2-s}{s}\,\frac{1}{(a_{\rm e}^{(0)}-v_{\rm e}^{(0)})(a_{\rm f}^{(0)}-v_{\rm f}^{(0)})} \\
\times\left[q_{\rm e}^{(1)}q_{\rm f}^{(0)}+q_{\rm f}^{(1)}q_{\rm e}^{(0)}-p_{\rm f}^{(1)}q_{\rm e}^{(0)}\frac{v_{\rm f}^{(0)}}{a_{\rm f}^{(0)}}-p_{\rm e}^{(1)}q_{\rm f}^{(0)}\frac{v_{\rm e}^{(0)}}{a_{\rm e}^{(0)}}-q_{\rm e}^{(0)}q_{\rm f}^{(0)}\frac{\Sigma_{\gamma\gamma}^{(1)}}{s}+\text{boxes}\right],
\end{aligned} \tag{17}$$

$$\kappa_{\rm e,f}(s) = \kappa_{\rm Z}^{\rm e,f}(s) + \frac{M_{\rm Z}^2-s}{s}\left[\frac{q_{\rm e,f}^{(0)}}{a_{\rm e,f}^{(0)}-v_{\rm e,f}^{(0)}}\,\frac{p_{\rm f,e}^{(1)}}{a_{\rm f,e}^{(0)}}+\text{boxes}\right], \tag{18}$$

$$\kappa_{\rm Z}^{\rm f}(s) = \kappa_{\rm Z}^{\rm f}(M_{\rm Z}^2) + (s-M_{\rm Z}^2)\,\frac{\hat{a}_{\rm f}^{(1)\prime}(M_{\rm Z}^2)\,v_{\rm f}^{(0)}-\hat{v}_{\rm f}^{(1)\prime}(M_{\rm Z}^2)\,a_{\rm f}^{(0)}}{a_{\rm f}^{(0)}(a_{\rm f}^{(0)}-v_{\rm f}^{(0)})}. \tag{19}$$

From the pole expansion scheme one obtains in contrast to eqs. (17),(18)

$$\overline{\kappa}_{\rm ef}(s) = \overline{\kappa}_{\rm e}(s)\overline{\kappa}_{\rm f}(s) - \frac{M_{\rm Z}^2 - iM_{\rm Z}\Gamma_{\rm Z} - s}{s} \frac{1}{(a_{\rm e}^{(0)} - v_{\rm e}^{(0)})(a_{\rm f}^{(0)} - v_{\rm f}^{(0)})} \times \left[q_{\rm e}^{(1)} q_{\rm f}^{(0)} + q_{\rm f}^{(1)} q_{\rm e}^{(0)} - p_{\rm f}^{(1)} q_{\rm e}^{(0)} \frac{v_{\rm f}^{(0)}}{a_{\rm f}^{(0)}} - p_{\rm e}^{(1)} q_{\rm f}^{(0)} \frac{v_{\rm e}^{(0)}}{a_{\rm e}^{(0)}} - q_{\rm e}^{(0)} q_{\rm f}^{(0)} \frac{\Sigma_{\gamma\gamma}^{(1)}}{s} + \text{boxes} \right], \quad (20)$$

$$\overline{\kappa}_{\rm e,f}(s) = \overline{\kappa}_{\rm Z}^{\rm e,f}(s) + \frac{M_{\rm Z}^2 - iM_{\rm Z}\Gamma_{\rm Z} - s}{s} \left[\frac{q_{\rm e,f}^{(0)}}{a_{\rm e,f}^{(0)} - v_{\rm e,f}^{(0)}} \frac{p_{\rm f,e}^{(1)}}{a_{\rm f,e}^{(0)}} + \text{boxes} \right]. \quad (21)$$

with

$$\overline{\kappa}_{\rm f} = \kappa_{\rm f} \left[1 + \frac{c_{\rm W}^2}{s_{\rm W}^2} \left(\frac{\Gamma_{\rm W}^2}{M_{\rm W}^2} - \frac{\Gamma_{\rm Z}^2}{M_{\rm Z}^2} \right) \right], \quad (22)$$

$$\overline{\kappa}_{\rm ef} = \kappa_{\rm ef} \left[1 + \frac{c_{\rm W}^2}{s_{\rm W}^2} \left(\frac{\Gamma_{\rm W}^2}{M_{\rm W}^2} - \frac{\Gamma_{\rm Z}^2}{M_{\rm Z}^2} \right) \right]^2, \quad (23)$$

Note that for next-to-next-to-leading accuracy it is not necessary to distinguish between barred and un-barred symbols in the radiative corrections, since $\overline{M}_{\rm Z}^2 - M_{\rm Z}^2 = \mathcal{O}(\alpha^2)$.

From eqs. (17–21) one finds a difference for the derivation of the value of $\sin^2\theta_{\rm eff}^f$ between ZFITTER and the pole scheme:

$$\sin^2\theta_{\rm eff,ZFITTER}^f = s_{\rm W}^2 \,\mathrm{Re}\left\{\kappa_{\rm Z}^{\rm f}(M_{\rm Z}^2)\right\} \quad (24)$$

$$\sin^2\theta_{\rm eff,pole}^f = \overline{s}_{\rm W}^2 \,\mathrm{Re}\left\{\overline{\kappa}_{\rm Z}^{\rm f}(M_{\rm Z}^2)\right\} = \sin^2\theta_{\rm eff,ZFITTER}^f - \frac{\Gamma_{\rm Z}}{M_{\rm Z}} \frac{q_{\rm f}^{(0)}}{a_{\rm e}^{(0)}(a_{\rm f}^{(0)} - v_{\rm f}^{(0)})} \,\mathrm{Im}\{p_{\rm e}^{(1)}\} \quad (25)$$

with

$$\overline{s}_{\rm W}^2 = \left(1 - \frac{\overline{M}_{\rm W}^2}{\overline{M}_{\rm Z}^2}\right) = s_{\rm W}^2 \left[1 + \frac{c_{\rm W}^2}{s_{\rm W}^2} \left(\frac{\Gamma_{\rm W}^2}{M_{\rm W}^2} - \frac{\Gamma_{\rm Z}^2}{M_{\rm Z}^2} \right) \right]^{-1}. \quad (26)$$

A similar deviation is found for the contribution of the form factors $\kappa_{\rm ef}, \overline{\kappa}_{\rm ef}$ between the two schemes, which however cannot be expressed directly as a shift in $\sin^2\theta_{\rm eff}^f$.

In principle, an additional discrepancy arises from the box contributions. The massive boxes with Z and W boson exchange are included in ZFITTER at the one-loop level, which is sufficient for the next-to-next-to-leading order calculation in the pole scheme. Nevertheless, in (21) an extra term stemming from the box contributions arises, which is proportional to $iM_{\rm Z}\Gamma_{\rm Z}$. However, this term does not contribute to the squared matrix element since the massive boxes have no absorptive part[1].

[1] A special case is Bhabha scattering, $f = e$, where additional box and t-channel diagrams contribute. For the purpose of this work, the subtraction of these contributions has not been analyzed in detail, justified by the fact that the e^+e^- final state has a relatively small impact on the determination of the effective weak mixing angle at present. In general, a more careful analysis of this process should be done in the future.

Besides the contributions from s-channel photon exchange and boxes, the translation between the measured asymmetries and the effective weak mixing angle requires the subtraction of QED and QCD corrections to the external fermions.

In the left-right asymmetry, the effect of final state QED and QCD corrections and initial-final state QED interference cancels [36] up to next-to-next-to-leading order. Initial-state QED radiation can be treated through convolution with a radiator function and has been computed including the exact $\mathcal{O}(\alpha^2)$ corrections and higher-order leading contributions [37].

For the forward-backward asymmetry on the Z pole, the contribution from final-state virtual and soft photon radiation vanishes for massless external fermions [12, 36, 38]. This statement is valid up to corrections of the order $\mathcal{O}(\alpha\,\Delta E_\gamma/\sqrt{s})$, where ΔE_γ is the soft-photon cut-off, and terms of order $\mathcal{O}(\alpha\,m_f/\sqrt{s}$, where m_f is the final-state fermion mass. Nevertheless, the complete one-loop contributions to final-state radiation are known and taken into account in the extraction of the effective weak mixing angle [35]. The leading effect of final-state fermion masses of $\mathcal{O}(\alpha\,m_f/\sqrt{s})$ is also known and included [39], with the remaining effects of order $\mathcal{O}(\alpha^2\Delta E_\gamma/\sqrt{s})$, $\mathcal{O}(\alpha^2 m_f/\sqrt{s}$, $\mathcal{O}(\alpha\,m_f^2/s)$ being numerically negligible for the two-loop analysis for $\sin^2\theta^f_{\rm eff}$ under study here. Multiple hard final-state photon radiation is taken into account by Monte-Carlo methods, see e.g. [40], with a small numerical error. QCD final state effects are treated similarly to the QED contributions.

Interference of initial-final state photon radiation is also known up to order $\mathcal{O}(\alpha)$for the forward-backward asymmetry. For sufficiently loose soft-photon cut, $\Delta E_\gamma \gtrsim \Gamma_{\rm Z}$, the initial-final interference of soft and virtual photons at the Z pole is suppressed by the width $\Gamma_{\rm Z}$ of the Z boson [12,38], so that the $\mathcal{O}(\alpha^2)$ contribution is effectively of order $\mathcal{O}(\alpha^2\Gamma_{\rm Z}/M_{\rm Z})$, i.e. beyond the next-to-next-to-leading order corrections under study in this work. As before, initial-state radiation to the forward-backward asymmetry is included up to $\mathcal{O}(\alpha^2)$, and partially beyond, by means of a convolution. Thus while a complete next-to-next-to-leading order calculation of QED corrections to the forward-backward asymmetry is not available, the present treatment of QED corrections is sufficient for a two-loop analysis of $\sin^2\theta^f_{\rm eff}$. Nevertheless, a complete $\mathcal{O}(\alpha^2)$ calculation of QED effects would be desirable.

In summary, it was found that the treatment of non-resonant contributions in ZFITTER is not consistent with the pole scheme at next-to-next-to-leading order. As a result, the value of $\sin^2\theta^f_{\rm eff}$ needs to be corrected by a shift

$$s^2_{\rm W}\,\delta\kappa_{\rm f} = -\frac{\Gamma_{\rm Z}}{M_{\rm Z}}\,\frac{q^{(0)}_{\rm f}}{a^{(0)}_{\rm e}(a^{(0)}_{\rm f}-v^{(0)}_{\rm f})}\,\mathrm{Im}\{p^{(1)}_{\rm e}\}\,. \tag{27}$$

Numerically this shift amounts to $s^2_{\rm W}\,\delta\kappa_{\rm f} \approx 1.5\times10^{-6}$, well below the current experimental error of 1.7×10^{-4} [1]. Therefore, this shift will be neglected in the analysis in section 5. It was checked that a similar shift $\delta\kappa_{\rm ef}$ in the form factor $\kappa_{\rm ef}$ also leads to a negligible numerical effect on $\sin^2\theta^f_{\rm eff}$.

2.2 Renormalization

In this work the on-shell renormalization scheme is employed. It defines the mass parameters and coupling constants in close relation to physical observables. The renormalized squared

masses are defined as the real part of the propagator poles, while the external fields are renormalized to unity at the position of the poles. The electromagnetic charge is defined as the coupling strength of the electromagnetic vertex in the Thomson limit. Explicit expressions for the necessary counterterms can be found in Ref. [5].

As described in the previous section, the computation of radiative corrections to the effective weak mixing angle entails the calculation of loop contributions to the $Zf\bar{f}$ vertex. In principle this involves a field renormalization for the Z boson, which appears as an external particle of the vertex. Beyond one-loop order, the treatment of field renormalizations for unstable particles proves to be not straightforward [41]. However, in the calculation of $\sin^2\theta^f_{\rm eff}$ all occurrences of the Z boson field renormalization drop out between the vector and axial-vector form factors in eq. (14). The independence of $\sin^2\theta^f_{\rm eff}$ on the total normalization of the Z boson field strength can already be seen in eq. (1), where the effective weak mixing angle is defined through the ratio of vertex form factors.

While the on-shell counterterms cancel the UV-divergencies in the virtual loop corrections, all IR- and collinear divergencies drop out in the quantity $\sin^2\theta^f_{\rm eff}$, as explained in the previous section. The computation of the loop integrals is performed using dimensional regularization. With this regularization scheme, special care is needed for the treatment of the γ_5 matrix in triangle fermion sub-loops. A practical solution to this problem will be discussed in detail in section 3.3.

2.3 Preliminaries

Throughout the calculation of the two-loop corrections, the masses and Yukawa couplings of all fermions but the top quark are neglected. The quark mixing matrix is assumed to be diagonal. The vector and axial-vector components of the vertex corrections $\hat{z}_{{\rm f},\mu}$ were projected out by contraction with suitable projection operators,

$$\hat{v}_{\rm f}(k^2) = \frac{1}{2(2-D)k^2}\,{\rm Tr}[\gamma^\mu \not{p}_1\, \hat{z}_{{\rm f},\mu}(k^2)\, \not{p}_2], \tag{28}$$

$$\hat{a}_{\rm f}(k^2) = \frac{1}{2(2-D)k^2}\,{\rm Tr}[\gamma_5\,\gamma^\mu \not{p}_1\, \hat{z}_{{\rm f},\mu}(k^2)\, \not{p}_2], \tag{29}$$

where D is the space-time dimension and $p_{1,2}$ are the momenta of the external fermions. As a result, only scalar integrals remain after projection, but there are non-trivial structures of scalar products in the numerators of the integrals, which require further treatment.

3 Calculation of fermionic two-loop vertex diagrams

The computation of the two-loop corrections to the effective weak mixing angle can be divided into the calculation of the vertex loop contributions to the $Zf\bar{f}$ vertex and the on-shell counterterms. The latter involve two-loop vacuum and self-energy contributions, similar to the two-loop corrections to the W-boson mass [4, 5], while the former also contain

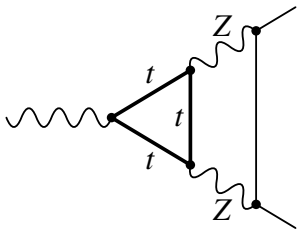

Figure 3: Example of a two-loop vertex diagram with a top-quark sub-loop.

two-loop vertex topologies as a new complication. The generic two-loop vertex diagrams with closed fermion loops are shown in Fig. 1.

The evaluation of the two-loop vertex contributions has been performed with two independent methods, in order to allow for a non-trivial check of the result. One method is based on large mass expansions for the diagrams involving internal top quark propagators and differential equations for the diagrams with only light fermions. The second method makes use of numerical integrations derived from dispersion relations and Feynman parameterizations.

3.1 Large top-quark mass expansions and analytical results

This approach divides the fermionic two-loop vertices in two categories: diagrams with internal top quark lines and diagrams that have only light fermion lines.

Observing that the ratio $x = M_{\mathrm{Z}}^2/m_{\mathrm{t}}^2 \sim 1/4$ is a small number, the top-quark contributions can be conveniently calculated by performing an expansion in x. The coefficients of this large-mass expansion decompose completely into one-loop integrals and two-loop vacuum integrals, for which analytical formulae are available in the literature [42].

An example of a typical scalar two-loop vertex diagram is shown in Fig. 3. The expansion of this diagram reads

$$x\,\frac{\zeta(2)}{3} + x^2\left(\frac{\zeta(2)}{12} - \frac{5}{36} + \frac{1}{12}\log x\right) + x^3\left(\frac{\zeta(2)}{45} - \frac{79}{1200} + \frac{1}{20}\log x\right) + \ldots \tag{30}$$

Numerically this amounts to

$$0.1483 - 0.0081 - 0.0019 + 0.0003 + \ldots \tag{31}$$

The excellent convergence of this series is typical for all diagrams that only contain neutral current exchange in the loop. Diagrams involving charged current exchange converge more slowly, which is an effect of the top-bottom mass splitting.

For this work, the large-mass expansion is executed up to order $x^5 = M_{\mathrm{Z}}^{10}/m_{\mathrm{t}}^{10}$, which yields an overall precision of 10^{-7}, by far sufficient for practical purposes. This high accuracy is a substantial improvement over the previous work in Ref. [23], where only the first two terms in an expansion for large m_{t} were calculated. Please note that the large-mass expansion was only used for the two-loop vertex diagrams. The two-loop counterterms, which in addition to the mass scales M_{W}, M_{Z} and m_{t} also involve the parameter M_{H}, were evaluated using one-dimensional integral representations as in Refs. [43, 44]. In principle it would also be possible to compute the counterterms using large-mass expansions. However, since in

$\mathrm{LF1}(p^2, m^2) =$ 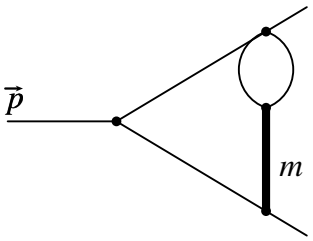

Figure 4: Example of scalar prototype integral. The thick line is massive with mass m, while the thin lines represent massless propagators.

general analytical results only exist for two-loop diagrams with up to two different scales, this would require a simultaneous expansion in m_t and M_H, as in Ref. [23, 45]. In order to obtain a precise result, the one-dimensional integral representations are more suitable instead.

The contributions with light fermions contain only the scales M_W and M_Z and are therefore functions of only one dimensionless variable $\omega = M_\mathrm{W}^2/M_\mathrm{Z}^2$. In this case it is possible to evaluate all contributions analytically using the differential equation method [47]. The final result is thus expressed through polylogarithms and generalized polylogarithms.

As a simple example consider the scalar integral in Fig. 4. Using integration-by-parts identities [48], the following differential equation can be derived:

$p^2 \frac{\mathrm{d}}{\mathrm{d}p^2}$ 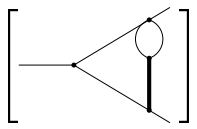 $= \frac{1}{2}\frac{p^2}{p^2+m^2}\Bigg((4-D)(4+5\frac{m^2}{p^2})$ 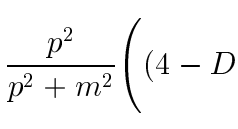

$+ (10-3D)$ 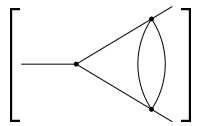 $- (2-D)$ 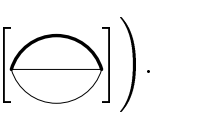 $\Bigg).$ (32)

Here the thick lines represent massive propagators with mass m and the thin lines denote massless propagators. Besides the integral LF1 under study, the differential equation involves a simpler scalar vertex integral and a vacuum integral on the right-hand side. Feeding in analytical expression for these integrals from the literature [42, 49], the differential equation can be solved in terms of Nielsen's polylogarithms [50]. The finite part of LF1 reads

$$\begin{aligned}\mathrm{LF1}(p^2, m^2) = {} & -\mathrm{Li}_2(-x)\big(-2 + 2\log(m^2) + 3\log(-x) + \log(1+x)\big) + 4\mathrm{Li}_3(-x) - S_{1,2}(-x) \\ & + \frac{1}{2}\log(1+x)\big[2\zeta_2 - \log(-x)\big((-4 + 4\log(m^2) + 2\log(-x) + \log(1+x)\big)\big],\end{aligned} \tag{33}$$

with $x = p^2/m^2$ and Nielsen's polylogarithm $S_{1,2}$ defined in Ref. [51]. The integral LF1 has also been calculated in Ref. [52]. However, some of the prototype integrals needed for this project have not been known before and were computed for the first time in this work. All integrals have been checked by different expansions in physical and unphysical regimes.

Several relevant integrals were also recently computed in Ref. [53]. However, their results were presented in terms of generalized harmonic polylogarithms, which in general involve numerical integrations for the numerical evaluation.

After performing the Dirac and Lorentz algebra for the relevant two-loop vertex diagrams, the result contains a large number of different scalar integrals with terms in the numerator

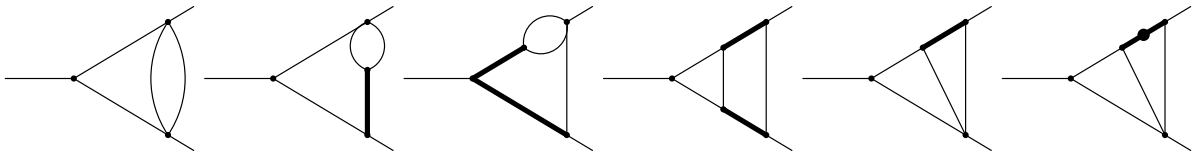

Figure 5: Scalar master integrals for diagrams with a light fermion loop. Thick lines indicate massive gauge boson propagators, while thin lines correspond to light fermions of photons, which are taken massless. The dot in the last diagram indicates that this propagator appears two times.

that cannot be cancelled against any of the propagators in the denominator. Here it is advantageous to perform an algebraic reduction to a minimal set of master integrals.

For the reduction to master integrals, the Laporta algorithm is used [54]. It is based on integration-by-parts [48] and Lorentz identities [55], which establish linear relations between scalar loop integrals. For a sufficiently large set of these relations, the linear equation system can be solved in order to express the more complicated integrals with non-trivial numerators in terms of a set of simple master integrals with unit numerators. This reduction algorithm is implemented in the C++ library IdSolver [56], which allows for a fast evaluation of linear systems involving several thousand equations.

The set of master integrals that appear within this calculation for the light fermion contributions is summarized in Fig. 5. Analytical expressions were found by the differential equation method for all but the fourth topology in Fig. 5, which was evaluated numerically.

3.2 Semi-numerical integrations

The second method employs numerical integrations for the master integrals. This technique is based on a dispersion representation of the one-loop self-energy function B_0,

$$B_0(p^2, m_1^2, m_2^2) = \int_{(m_1+m_2)^2}^{\infty} \mathrm{d}s \, \frac{\Delta B_0(s, m_1^2, m_2^2)}{s - p^2}, \tag{34}$$

$$\Delta B_0(s, m_1^2, m_2^2) = (4\pi\mu^2)^{4-D} \, \frac{\Gamma(D/2-1)}{\Gamma(D-2)} \, \frac{\lambda^{(D-3)/2}(s, m_1^2, m_2^2)}{s^{D/2-1}}, \tag{35}$$

where D is the space-time dimension and $\lambda(a,b,c) = (a-b-c)^2 - 4bc$. Using this relation, any scalar two-loop integral T with a self-energy sub-loop as in Fig. 6 (a) can be expressed as [43]

$$\begin{aligned} T_{N+1}(p_i; m_i^2) = &- \int_{s_0}^{\infty} \mathrm{d}s \, \Delta B_0(s, m_N^2, m_{N+1}^2) \\ &\times \int \mathrm{d}^4 q \, \frac{1}{q^2 - s} \, \frac{1}{(q+p_1)^2 - m_1^2} \cdots \frac{1}{(q+p_1+\cdots+p_{N-1})^2 - m_{N-1}^2}. \end{aligned} \tag{36}$$

Here the integral in the second line is a N-point one-loop function, and the integration over s is performed numerically. While in principle it is also possible to introduce dispersion

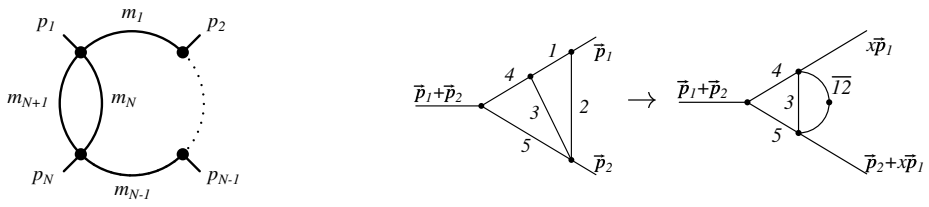

Figure 6: (a) General representation of a two-loop scalar diagram with self-energy sub-loop. (b) Reduction of triangle sub-loop to self-energy sub-loop by means of Feynman parameters.

relations for triangle sub-loops [44, 57], it is technically easier to reduce them to self-energy sub-loops by introducing Feynman parameters [58],

$$\begin{aligned} [(q+p_1)^2 - m_1^2]^{-1}\,[(q+p_2)^2 - m_2^2]^{-1} &= \int_0^1 \mathrm{d}x\,[(q+\bar{p})^2 - \overline{m}^2]^{-2} \\ \bar{p} = x\,p_1 + (1-x)p_2, \qquad \overline{m}^2 &= x\,m_1^2 + (1-x)m_2^2 - x(1-x)(p_1-p_2)^2. \end{aligned} \tag{37}$$

This is indicated diagrammatically in Fig. 6 (b). The integration over the Feynman parameters is also performed numerically. As a result, all master integrals for the vertex topologies can be evaluated by at most 3-dim. numerical integrations.

The basic scalar two-loop integrals might contain UV- and IR-divergencies. These need to be subtracted before the numerical integration can be carried out. An elegant method to remove the divergencies is by subtracting a term from the integrand that can be integrated analytically. This can be illustrated by the subtraction of UV divergencies in the following example:

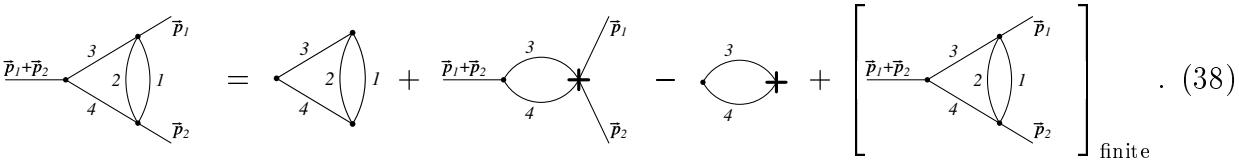

(38)

The UV divergent part of the two-loop vertex diagram can be identified by the sum of the same diagram with zero external momenta and the contribution from sub-loop renormalization. The first term corresponds to a two-loop vacuum diagram for which analytical formulae are available in the literature [42], while the second and third terms are products of one-loop functions,

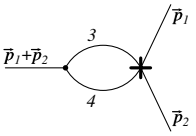

$$= B_0\left((p_1+p_2)^2, m_3^2, m_4^2\right) \times B_0\left(m_4^2, m_1^2, m_2^2\right), \tag{39}$$

$$= B_0\left(0, m_3^2, m_4^2\right) \times B_0\left(m_4^2, m_1^2, m_2^2\right). \tag{40}$$

Here the momentum scale m_4^2 for the sub-loop counterterm was chosen to be able to handle the case $0 = m_1 = m_2 \neq m_4$. Subtracting these terms in the integrand of the two-loop vertex integral results in a finite contribution, that can be integrated numerically,

$$\left[\quad\right]_{\text{finite}} = -\int_{(m_1+m_2)^2}^{\infty} \mathrm{d}s\ \Delta B_0(s, m_1^2, m_2^2) \times \left[C_0\left((p_1+p_2)^2, p_1^2, p_2^2, m_3^2, m_4^2, s\right) - C_0\left(0,0,0,m_3^2,m_4^2,s\right) + \frac{1}{s-m_4^2}\left[B_0\left((p_1+p_2)^2, m_3^2, m_4^2\right) - B_0\left(0, m_3^2, m_4^2\right)\right]\right]. \tag{41}$$

For all other two-loop vertex master integrals, the divergent parts can be removed in a similar fashion.

As before, the reduction of integrals with irreducible numerators to a small set of master integrals is accomplished by using integration-by-parts and Lorentz-invariance identities, which were implemented in an independent realization of the Laporta algorithm within Mathematica.

3.3 Diagrams with fermion loop triangles and treatment of γ_5

Diagrams with a fermion triangle sub-loop pose a special problem in conjunction with the use of dimensional regularization. The fermion triangle loop involves terms like

$$\mathrm{Tr}(\gamma^\alpha\gamma^\beta\gamma^\gamma\gamma^\delta\gamma_5) = 4i\,\epsilon^{\alpha\beta\gamma\delta}, \tag{42}$$

which cannot be extended to D dimensions simultaneously with the anti-commutation rule $\{\gamma_\mu, \gamma_5\} = 0$. However, renormalizability of the Standard Model demands that terms originating from expressions like eq. (42) are always UV-finite in any two-loop diagram. As a consequence, the diagrams with a fermion triangle loop can be treated in two steps [4]: First the complete diagrams are calculated using naive dimensional regularization with anti-commuting γ_5, where the trace in eq. (42) is zero. The finite contributions resulting in epsilon tensors are computed independently in four dimensions, and finally the two contributions are added.

An additional complication arises from diagrams with internal photon lines and massless external fermions, Fig. 7, which could give rise to soft-collinear divergencies. While these soft and collinear divergencies are spurious singularities, thus dropping out in the total result, they result in inconsistencies if dimensional regularization is used. In this case the contributions involving epsilon tensors from the fermion triangle cannot be treated consistently in four dimensions anymore.

In this work, the soft and collinear divergencies in these diagrams were instead regulated with a photon mass. In the complete result, the limit of zero photon mass was taken by means of an expansion, involving a careful treatment in the mixed Sudakov/threshold regime. The result for the diagrams with two photons has been checked against Ref. [46].

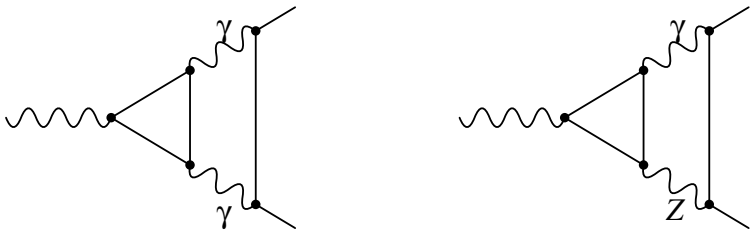

(a) (b)

Figure 7: Diagrams with fermion triangle sub-loops and soft-collinear divergencies.

3.4 Checks

The master integrals have been checked with published results where applicable [52,53]. Some master integrals were tested by means of Mellin-Barnes representations, see also [59–61], and with a low-momentum expansion. In addition, complete diagrams were tested with a low-momentum expansion. In the comparison of the two methods explained in the previous sections, complete agreement was found.

4 Calculation of bosonic two-loop vertex diagrams

As explained in the previous chapter, the calculation of the bosonic two-loop corrections fall into two categories, the bare vertex diagrams and the on-shell renormalization terms. The computation of the renormalization counterterms has been established previously [5,6], whereas the calculation of the vertex diagrams will be addressed here. In our case, this involves massive two-loop three-point function with one massive external leg and up to three different mass scales.

Contrary to the fermionic corrections, the bosonic diagrams do not depend on the top quark. On the other hand, there is a dependence on the Higgs boson mass, which is not a fixed parameter and can assume a broad range of values. Due to complexity of the problem with several hundred diagrams and many more different algebraic integral structures, the calculation cannot be performed in a straightforward way with any known computational method. Here the task is approached by using an expansion in the various parameters in order to obtain a result expressed through single scale integrals, which have to be evaluated numerically in a final step.

In a first step, we apply an expansion in the difference of the masses of the W and Z bosons, where the expansion parameter is just s_{W}^2. Since there are diagrams where there is a threshold when $M_{\mathrm{W}} = M_{\mathrm{Z}}$, the appearance of divergences at higher orders in the expansion is inevitable. In this case, we apply the method of expansions by regions, see [62]. In this approach, one analyzes the momentum regions which can contribute to the integral and expands the integrand in each region with a different expansion parameter. The two regions that contribute to the result come from the *ultrasoft momenta*, $q_{1,2} \sim s_{\mathrm{W}}^2 M_{\mathrm{Z}}$, and *hard momenta*, $q_{1,2} \sim M_{\mathrm{Z}}$, where $q_{1,2}$ are the loop momenta. Then the reduction to the set of master integrals proceeds with Integration-By-Parts identities [48] solved with the Laporta

algorithm [54] as implemented in the *IdSolver* library [56].

The $M_{\rm H}$ dependence is treated in two regimes. For low values of $M_{\rm H}$ an expansion in the mass difference between $M_{\rm H}$ and $M_{\rm Z}$ is used, with the expansion parameter defined to be

$$s_{\rm H}^2 = 1 - \frac{M_{\rm H}^2}{M_{\rm Z}^2}, \tag{43}$$

where this time no non-trivial thresholds are encountered. It is found that a good precision is achieved by performing the expansion to the sixth order in $s_{\rm W}^2$ and $s_{\rm H}^2$. The second regime is for large values of $M_{\rm H} \gg M_{\rm Z}$, where a large mass expansion [62] is used.

The resulting single scale master integrals are treated with various methods, usually with two or three different ones for test purposes. Most integrals can be obtained with numerical integrations based on dispersion relations as described in section 3.2. The advantage of this method is that with reasonable investment of computer time, it can be pushed to high precision, which is required since large numerical cancellations are observed between individual integrals. Diagrams of simpler topologies can also be evaluated with differential equations [63, 64] and large mass expansions. For more complicated topologies, Mellin-Barnes representations are employed, using the MB package [59], see also [60, 61]. After simplification, the Mellin-Barnes representations can be evaluated by numerical integrations or infinite series. In principle, this method could be used for all scalar integrals, however, depending on the mass configuration, the integration and/or the series evaluation does not converge. The convergence behavior can be improved by rotating the integration contours into the complex plane, but this also solves the problem only in a few cases. Whenever possible the results were cross-checked with sector decomposition [65].

The reduction to master integrals can occasionally can produce spurious $1/(D-4)$ poles in the coefficients of some master integrals. In principle, this problem can be avoided by choosing an appropriate basis of master integrals, at the expense, however, that some of these integrals are more complicated. Here, on the other hand, a basis was chosen that introduces only relatively few spurious poles, but in front of simple integrals. Since it is advantageous to check the cancellation of divergencies exactly, it was thus necessary to evaluate the finite pieces of some master integrals analytically. These integrals are presented in Ref. [66].

As a final algebraic check of the whole procedure, the cancellation of the gauge parameter dependence in a general covariant R_ξ gauge was verified. Due to the enormous complexity of the intermediate expressions, this test was only possible for the first orders in the expansion, but nevertheless allowed a non-trivial cross-check between different diagram topologies.

5 Numerical Results

In order to arrive at a precise prediction for the effective weak mixing angle, the electroweak corrections of one- and two-loop order are combined with one- and two-loop QCD corrections [16, 17], and leading three-loop corrections of order $\mathcal{O}(G_\mu^3 m_{\rm t}^6)$ and $\mathcal{O}(G_\mu^2 \alpha_{\rm s} m_{\rm t}^4)$ [14]. Other higher-order corrections to the rho parameter of order $\mathcal{O}(G_\mu^3 M_{\rm H}^4)$ [15] and $\mathcal{O}(G_\mu m_t^2 \alpha_{\rm s}^3)$ [18] are very small (for $M_{\rm H} < 1$ TeV) and thus not included in the numerical analysis. The result

Input parameter	Value
$M_{\rm W}$	80.404 ± 0.030 GeV
$M_{\rm Z}$	91.1876 ± 0.0021 GeV
Γ_Z	2.4952 GeV
m_t	172.5 ± 2.3 GeV
m_b	4.85 GeV
$\Delta\alpha(M_{\rm Z}^2)$	0.05907 ± 0.00036
$\alpha_s(M_{\rm Z})$	0.119 ± 0.002
G_μ	1.16637×10^{-5} GeV^{-2}

Table 1: Experimental input parameters used in the numerical evaluation; from Refs. [67,68].

is expressed as a perturbative expansion in α, not G_μ.Instead, all higher-order reducible contributions, that arise from terms proportional to $\Delta\alpha$ and $\Delta\rho$, are included explicity at the given loop order in the computation. A finite b quark mass was retained in the $\mathcal{O}(\alpha)$ and $\mathcal{O}(\alpha\alpha_{\rm s})$ contributions, but neglected in all higher-order terms.

In Tab. 2, the effects of the various loop contributions on the vertex form factor $\Delta\kappa$ are shown for the input parameters in Tab. 1. $\Delta\alpha$ is defined as the real part of the shift of the photon vacuum polarization function $\Pi(q^2)$ between $q^2 = 0$ and $q^2 = M_{\rm Z}^2$ that stems from light fermions,

$$\Delta\alpha = \mathrm{Re}\left\{\Pi_{\rm lf}(0) - \Pi_{\rm lf}(M_{\rm Z}^2)\right\}, \qquad \Pi(q^2) = \Pi_{\rm lf}(q^2) + \Pi_{\rm rest}(q^2). \tag{44}$$

It is important to note that the experimental values for the W and Z boson masses in Tab. 1 correspond to a Breit-Wigner parametrization with a running width, that have to be translated to the pole mass scheme used in the loop calculations [4]. In effect, this translation results in a downward shift [69] of $M_{\rm Z}$ by 34 MeV and $M_{\rm W}$ by 28 MeV, respectively.

As evident from the table, the fermionic and bosonic contributions to $\Delta\kappa$ are of the same magnitude. This changes, however, when expressing the result through the Fermi constant G_μ as input parameter. For this, the corresponding loop corrections, Δr, to the W boson mass need to be incorporated,

$$M_{\rm W}^2\left(1 - \frac{M_{\rm W}^2}{M_{\rm Z}^2}\right) = \frac{\pi\alpha}{\sqrt{2}G_\mu}\left(1 + \Delta r\right). \tag{45}$$

The inclusion of the corrections to $M_{\rm W}$ lead to an enhancement of the fermionic two-loop corrections to $\sin^2\theta_{\rm eff}^{\rm lept}$, but to a partial cancellation between the bosonic two-loop corrections in $\Delta\kappa$ and Δr. The effect of the different loop orders in $\sin^2\theta_{\rm eff}^{\rm lept}$with G_μ as input parameter is summarized in Fig. 8. The figure shows that the contribution from the fermionic two-loop

$M_{\rm H}$ [GeV]	$\mathcal{O}(\alpha)$ [10^{-4}]	$\mathcal{O}(\alpha^2)_{\rm ferm}$	$\mathcal{O}(\alpha^2)_{\rm bos}$	$\mathcal{O}(\alpha\alpha_{\rm s})$	$\mathcal{O}(\alpha\alpha_{\rm s}^2)$	$\mathcal{O}(\alpha^2\alpha_{\rm s}m_{\rm t}^4)$	$\mathcal{O}(\alpha^3 m_{\rm t}^6)$	red.
100	413.33	1.07	-0.74	-35.58	-7.25	1.15	0.14	0.69
200	394.02	-0.32	-0.47	-35.58	-7.25	1.90	0.07	0.70
600	354.06	-2.89	0.17	-35.58	-7.25	3.70	0.08	0.72
1000	333.16	-2.61	1.11	-35.58	-7.25	4.53	0.91	0.72

Table 2: Loop contributions to $\Delta\kappa$ with fixed $M_{\rm W}$ as input parameter as a function of the Higgs mass $M_{\rm H}$. Here "red." corresponds to reducible three-loop contributions stemming from $\Delta\alpha$ and $\Delta\rho$.

corrections amount to roughly $\sim 10^{-3}$, while the resulting effect of the bosonic two-loop corrections is about or less than $\sim 10^{-5}$, so that the two curves for $\mathcal{O}(\alpha+\alpha\alpha_{\rm s}+\alpha\alpha_{\rm s}^2+\alpha_{\rm ferm}^2)$ and $\mathcal{O}(\alpha+\alpha\alpha_{\rm s}+\alpha\alpha_{\rm s}^2+\alpha_{\rm ferm}^2+\alpha_{\rm bos}^2)$ practically overlap.

For the analysis in the following sections, the new full result always includes terms of the orders α, α^2, $\alpha\alpha_{\rm s}$, $\alpha\alpha_{\rm s}^2$, $\alpha^2\alpha_{\rm s}m_{\rm t}^4$ and $\alpha^3 m_{\rm t}^6$,

$$\sin^2\theta_{\rm eff}^{\rm lept}\big|_{\rm full} = \sin^2\theta_{\rm eff}^{\rm lept}\big|_{\alpha+\alpha^2+\alpha\alpha_{\rm s}+\alpha\alpha_{\rm s}^2+\alpha^2\alpha_{\rm s}m_{\rm t}^4+\alpha^3 m_{\rm t}^6}. \tag{46}$$

5.1 Comparison with previous results

The most precise previous result for the two-loop electroweak corrections to $\sin^2\theta_{\rm eff}^{\rm lept}$ was obtained from the calculation of the next-to-leading term $\mathcal{O}(G_\mu^2 m_{\rm t}^2 M_{\rm Z}^2)$ in an expansion for large values of the top-quark mass $m_{\rm t}$ [23]. The impact of the new result, as defined in eq. (46), is shown in Tab. 3 (a) by comparing with the previous result as in the fitting formula in Ref. [70] and in the implementation of the program ZFITTER 5.10 (and later versions) [35].

A more detailed analysis reveals that there are several sources for the deviations listed in Tab. 3 (a). First of all, there is the effect of the truncated series expansion in $m_{\rm t}^{-2}$, which was evaluated only up to order $m_{\rm t}^2$ in Ref. [23]. In addition, the genuine light-fermion two-loop contributions were not included in that work. Moreover, the implementation of the correction form factor Δr to the W mass and the parametrization with G_μ instead of α in Ref. [23] introduces higher-order terms that can be sizeable. Here it is important to note that the OSI scheme in Ref. [23], which is the basis for the implementation of these corrections in ZFITTER, uses the $\overline{\rm MS}$ definition for $\Delta\rho$, which is numerically larger than the leading $m_{\rm t}^2$ term, so that the resummation effects of $\Delta\rho^{\overline{\rm MS}}$ are rather large. Finally, ZFITTER versions before 6.40 use an outdated implementation of the QCD corrections. Since all these contributions are non-negligible at the current level of precision, it is interesting to study them separately.

In particular, using the results of section 3.1 the effect of the truncated top-mass expan-

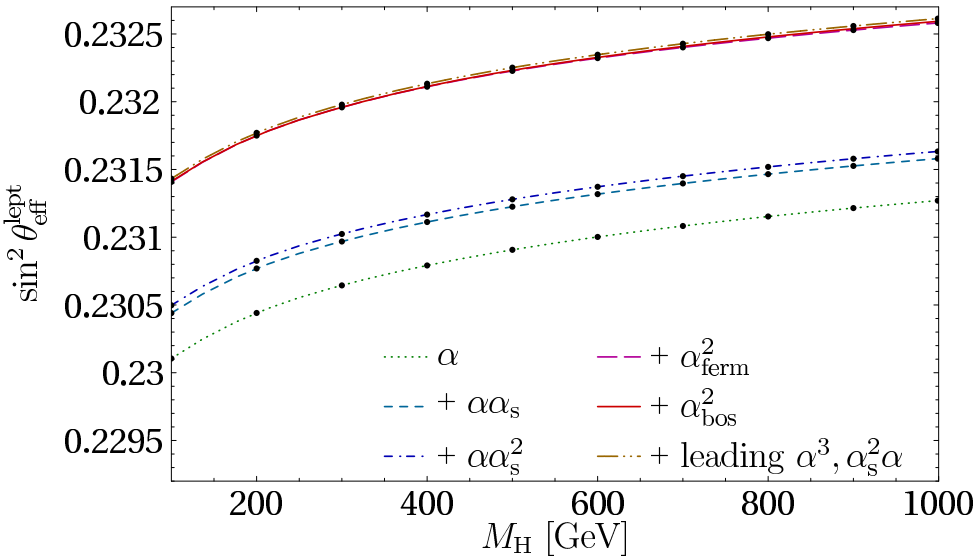

Figure 8: Contribution of several orders of radiative corrections to the effective leptonic weak mixing angle $\sin^2\theta^{\rm lept}_{\rm eff}$ as a function of the Higgs mass $M_{\rm H}$. The tree-level value is not shown.

sion is shown in Tab. 3 (b)[2]. It turns out that the expansion converges quite well for realistic values of $m_{\rm t}$ and $M_{\rm H}$. However, the terms beyond the order $m_{\rm t}^2$ induce a difference of 4.3% in the two-loop corrections with top-bottom loops, corresponding to a shift of about 0.2×10^{-4} in $\sin^2\theta^{\rm lept}_{\rm eff}$, which is roughly a quarter of the total difference reported in Tab. 3 (a). As a cross-check, also the result for very large values of $m_{\rm t}$ and $M_{\rm H}$ are shown in Tab. 3 (b), to illustrate that in this case the series converges much faster.

5.2 Error estimate

While the inclusion of the fermionic two-loop corrections is a substantial improvement of the prediction of $\sin^2\theta^{\rm lept}_{\rm eff}$ in the Standard Model, uncertainties from missing higher order contributions can still be sizeable. Here we try to give an estimate of the error induced by these unknown contributions. The most relevant missing higher order contributions are corrections of the order $\mathcal{O}(\alpha^2\alpha_{\rm s})$ beyond the leading $m_{\rm t}^4$ term, $\mathcal{O}(\alpha^3)$ beyond the leading $m_{\rm t}^6$ term and $\mathcal{O}(\alpha\alpha_{\rm s}^3)$. Since the final prediction for $\sin^2\theta^{\rm lept}_{\rm eff}$ is based on G_μ as input, the loop effects in the both quantities Δr (for the computation of $M_{\rm W}$) and $\Delta\kappa$ (for the Zl^+l^- vertex corrections) need to be considered.

When combining the two form factors, it turns out that there are some cancellations between the known corrections to $M_{\rm W}$ and the Z vertex. It is expected that similar cancellations occur when adding an additional QCD loop, since QCD corrections enter with the same relative sign in the corrections to $M_{\rm W}$ and the Z vertex. Since the dominant missing

[2] As a by-product of this comparison, we found a typo in Ref. [45], where a term $\frac{3}{2}m_{\rm t}^2/(M_{\rm Z}^2 s_{\rm W}^2)\log c_{\rm W}^2$ is missing in the expression for $M_{\rm H} \gg m_{\rm t}$.

(a)

$M_{\rm H}$ [GeV]	$\left[\Delta \sin^2\theta^{\rm lept}_{\rm eff}\right]_{\rm ZFITTER}$ [10^{-4}]	$\left[\Delta \sin^2\theta^{\rm lept}_{\rm eff}\right]_{[70]}$ [10^{-4}]
100	-0.45	-0.40
200	-0.69	-0.72
600	-1.17	-0.94
1000	-1.60	-1.28

(b)

$m_{\rm t}$, $M_{\rm H}$ [GeV]	$\Delta[m_{\rm t}^4]$	$\Delta[m_{\rm t}^2]$	$\Delta[m_{\rm t}^{-4}]$
175,400	20%	4.3%	0.02%
800,1800	5%	1.9%	0.00002%

Table 3: (a) Difference between the new result of eq. (46) and the previous result from Ref. [23], as implemented in ZFITTER (left column) and from the fitting formula in Ref. [70] (right column). (b) Convergence of the expansion in $m_{\rm t}^{-2}$ for the two-loop diagrams with top propagators. Here $\Delta[m_{\rm t}^k] = [\sin^2\theta^{\rm lept}_{\rm eff}]_{(\alpha^2 m_{\rm t}^k)}/[\sin^2\theta^{\rm lept}_{\rm eff}]_{(\alpha^2{\rm exact})} - 1$ is the relative difference between the exact and the expanded result at the given order.

	Geometric progression	Scale dependence	Leading $m_{\rm t}$ terms
$\mathcal{O}(\alpha^2\alpha_{\rm s})$ beyond leading $m_{\rm t}^4$	$3.3\ldots2.8\times10^{-5}$	$0.8\ldots2.1\times10^{-5}$	$1.2\ldots4.3\times10^{-5}$
$\mathcal{O}(\alpha\alpha_{\rm s}^3)$	$1.5\ldots1.4$	$0.3\ldots0.2$	
$\mathcal{O}(\alpha^3)$ beyond leading $m_{\rm t}^6$	$2.5\ldots3.5$		$0.3\ldots0.8$
Sum	$4.4\ldots4.7\times10^{-5}$		

Table 4: Estimation of the uncertainty from different higher order contributions for $\sin^2\theta^{\rm lept}_{\rm eff}$, with the quadratic sum of all error sources. Where applicable, two or three different methods for the error estimate have been used.

higher order effects are contributions with an additional QCD loop, it is assumed in the following that these cancellations are natural and it is justified to study the theoretical error of both quantities Δr and $\Delta\kappa$ in conjunction.

A simple method to estimate the higher order uncertainties is based on the assumption that the perturbation series follows roughly a geometric progression. This presumption implies relations like

$$\mathcal{O}(\alpha^2\alpha_{\rm s}) = \frac{\mathcal{O}(\alpha^2)}{\mathcal{O}(\alpha)}\,\mathcal{O}(\alpha\alpha_{\rm s}). \tag{47}$$

From this one obtains the error estimates in the second column of Tab. 4 for the different higher order contributions, which are given for a range of the Higgs $M_{\rm H}$ mass between 10 GeV and 1000 GeV. To account for possible deviations from the geometric series behavior, an ad-hoc overall factor $\sqrt{2}$ was included in all error determined via this method.

Alternatively, the error from a higher-order QCD loop can be assessed by varying the scale of the strong coupling constant $\alpha_{\rm s}$ or the top-quark mass $m_{\rm t}$ in the $\overline{\rm MS}$ scheme in the highest

available perturbation order. By varying thus the scale μ of $m_{\mathrm{t},\overline{\mathrm{MS}}}$ in the $\mathcal{O}(\alpha^2)$ contributions between $m_{\mathrm{t}}^2/2 < \mu^2 < 2m_{\mathrm{t}}^2$ one obtains an error estimate for the $\mathcal{O}(\alpha^2\alpha_{\mathrm{s}})$ contributions between 0.1 and 3.9×10^{-5}, depending on the value of M_{H} for 10 GeV $< M_{\mathrm{H}} <$ 1000 GeV. Similarly, by varying $\alpha_{\mathrm{s}}(\mu)$ in the $\mathcal{O}(\alpha\alpha_{\mathrm{s}}^2)$ corrections between $m_{\mathrm{t}}^2/2 < \mu^2 < 2m_{\mathrm{t}}^2$ leads to an error estimate for the $\mathcal{O}(\alpha\alpha_{\mathrm{s}}^3)$ contributions of less than 10^{-6}, see Tab. 4.

An independent third estimate of the error of the $\mathcal{O}(\alpha^2\alpha_{\mathrm{s}})$ and $\mathcal{O}(\alpha^3)$ contributions can be obtained from the existing leading terms in the expansion for large top quark mass. Experience from the $\mathcal{O}(\alpha^2)$ corrections suggests that for moderate values of M_{H}, the leading m_{t}-term and the remaining non-leading terms are of similar order. These contributions are shown in the last column of Tab. 4.

As evident from the table, all methods give results of similar order of magnitude, while the geometric progression method tends to lead to the largest error evaluation. The total estimated error is therefore computed by summing in quadrature the error from different contributions obtained by this method. It is found to amount to $\delta_{\mathrm{th}}\sin^2\theta_{\mathrm{eff}}^{\mathrm{lept}} = 4.7 \times 10^{-5}$.

5.3 Parametrization formulae

Following Ref. [26], the numerical results are expressed in terms of a fitting formula, which reproduces the exact calculation with maximal and average deviations of 4.5×10^{-6} and 1.2×10^{-6}, respectively, as long as the input parameters stay within their 2σ ranges and the Higgs boson mass in the range 10 GeV $\leq M_H \leq$ 1 TeV. For the sake of comparability with the result of Ref. [26], the slightly outdated central values for the experimental input parameters used there are also kept in the formula

$$\begin{aligned}\sin^2\theta_{\mathrm{eff}}^f = {} & s_0 + d_1 L_H + d_2 L_H^2 + d_3 L_H^4 + d_4(\Delta_H^2 - 1) + d_5\Delta_\alpha \\ & + d_6\Delta_t + d_7\Delta_t^2 + d_8\Delta_t(\Delta_H - 1) + d_9\Delta_{\alpha_{\mathrm{s}}} + d_{10}\Delta_Z,\end{aligned} \tag{48}$$

with

$$\begin{aligned} L_H &= \log\left(\frac{M_H}{100\ \mathrm{GeV}}\right), \qquad \Delta_H = \frac{M_H}{100\ \mathrm{GeV}}, \qquad \Delta_\alpha = \frac{\Delta\alpha}{0.05907} - 1, \\ \Delta_t &= \left(\frac{m_t}{178.0\ \mathrm{GeV}}\right)^2 - 1, \quad \Delta_{\alpha_{\mathrm{s}}} = \frac{\alpha_{\mathrm{s}}(M_{\mathrm{Z}})}{0.117} - 1, \quad \Delta_Z = \frac{M_{\mathrm{Z}}}{91.1876\ \mathrm{GeV}} - 1. \end{aligned} \tag{49}$$

The values of the coefficients for the effective leptonic weak mixing angle $\sin^2\theta_{\mathrm{eff}}^{\mathrm{lept}}$ are given in the second column of Tab. 5. This parametrization includes all relevant known corrections at this time, as in eq. (46).

For some purposes, it is however useful to have a numerical result for the two-loop electroweak form factors $\Delta\kappa$ and Δr alone. For $\Delta\kappa$, the following parametrization provides a good approximation,

$$\Delta\kappa^{(\alpha^2)} = \Delta\alpha\,\Delta\kappa^{(\alpha)} + \Delta\kappa_{\mathrm{rem}}^{(\alpha^2)}, \tag{50}$$

$$\begin{aligned}\Delta\kappa_{\mathrm{rem}}^{(\alpha^2)} = {} & k_0 + k_1 L_H + k_2 L_H^2 + k_3 L_H^4 + k_4(\Delta_H^2 - 1) + k_5\Delta_t + k_6\Delta_t^2 + k_7\Delta_t L_H \\ & + k_8\Delta_W + k_9\Delta_W\Delta_t + k_{10}\Delta_Z,\end{aligned} \tag{51}$$

with

$$\Delta_W = \frac{M_{\rm W}}{80.404\ {\rm GeV}} - 1. \tag{52}$$

From a fit to the exact computation, the coefficients are obtained as

$$\begin{aligned} &k_0 = -0.002711, \quad k_1 = -3.12 \times 10^{-5}, \quad k_2 = -4.12 \times 10^{-5}, \quad k_3 = 5.28 \times 10^{-6}, \\ &k_4 = 3.75 \times 10^{-6}, \quad k_5 = -5.16 \times 10^{-3}, \quad k_6 = -2.06 \times 10^{-3}, \quad k_7 = -2.32 \times 10^{-4}, \\ &k_8 = -0.0647, \qquad k_9 = -0.129, \qquad k_{10} = 0.0712. \end{aligned} \tag{53}$$

This reproduces the exact result for $\Delta\kappa^{(\alpha^2)}$ with maximal deviations of 1.8×10^{-5} for 10 GeV $\leq M_H \leq$ 1 TeV and the other input parameters in their 2σ ranges. This error in $\Delta\kappa$ corresponds to an error of 4×10^{-6} for $\sin^2\theta^{\rm lept}_{\rm eff}$. Since the experimental values for the top quark mass and the W-boson mass might change substantially with future updates of measurements from the Tevatron and the LHC, it is useful to see how well the fitting formula works for larger ranges of these two parameters. If the top quark mass and the W-boson mass vary within 4σ of their current experimental uncertainty, the formula eq. (50) is still accurate to 3.6×10^{-5}, corresponding to an error of 8×10^{-6} for $\sin^2\theta^{\rm lept}_{\rm eff}$.

Similarly, for Δr, the numerical result can be cast into the form

$$\Delta r^{(\alpha^2)} = (\Delta\alpha)^2 + 2\Delta\alpha\,\Delta r^{(\alpha)} + \Delta r^{(\alpha^2)}_{\rm rem}, \tag{54}$$

$$\begin{aligned} \Delta r^{(\alpha^2)}_{\rm rem} = {} & r_0 + r_1 L_H + r_2 L_H^2 + r_3 L_H^4 + r_4(\Delta_H^2 - 1) + r_5\Delta_t + r_6\Delta_t^2 + r_7\Delta_t L_H \\ & + r_8\Delta_W + r_9\Delta_W\Delta_t + r_{10}\Delta_Z, \end{aligned} \tag{55}$$

where

$$\begin{aligned} &r_0 = 0.003354, \qquad r_1 = -2.09 \times 10^{-4}, \quad r_2 = 2.54 \times 10^{-5}, \quad r_3 = -7.85 \times 10^{-6}, \\ &r_4 = -2.33 \times 10^{-6}, \quad r_5 = 7.83 \times 10^{-3}, \quad r_6 = 3.38 \times 10^{-3}, \quad r_7 = -9.89 \times 10^{-6}, \\ &r_8 = 0.0939, \qquad r_9 = 0.204, \qquad r_{10} = -0.103. \end{aligned} \tag{56}$$

This agrees with the exact result within maximal deviations of 2.7×10^{-5} for 10 GeV $\leq M_H \leq$ 1 TeV and the other input parameters in their 2σ ranges, corresponding to an error of 0.4 MeV for $M_{\rm W}$ and 8×10^{-6} for $\sin^2\theta^{\rm lept}_{\rm eff}$. For the top quark mass and the W-boson mass varying in their 4σ ranges, the formula eq. (54) is accurate to 4.3×10^{-5}, corresponding to an error of 0.65 MeV for $M_{\rm W}$ and 12.5×10^{-6} for $\sin^2\theta^{\rm lept}_{\rm eff}$.

5.4 Results for other fermion flavors

The results presented in the previous sections and in Refs. [26, 27] give the effective weak mixing angle $\sin^2\theta^{\rm lept}_{\rm eff}$ defined for the leptonic Zl^+l^- vertex. For the $Zf\bar{f}$ vertex with other light flavors $f = \nu, u, d$ in the final state, there are small but non-zero differences with respect to the leptonic effective weak mixing angle. In this section, results are given for $\sin^2\theta^{f}_{\rm eff}$ for different final state fermions except b-quarks. For the $b\bar{b}$ final state, the two-loop

f	e,μ,τ	$\nu_{e,\mu,\tau}$	u,c	d,s
s_0	0.2312527	0.2308772	0.2311395	0.2310286
d_1 $[10^{-4}]$	4.729	4.713	4.726	4.720
d_2 $[10^{-5}]$	2.07	2.05	2.07	2.06
d_3 $[10^{-6}]$	3.85	3.85	3.85	3.85
d_4 $[10^{-6}]$	−1.85	−1.85	−1.85	−1.85
d_5 $[10^{-2}]$	2.07	2.06	2.07	2.07
d_6 $[10^{-3}]$	−2.851	−2.850	−2.853	−2.848
d_7 $[10^{-4}]$	1.82	1.82	1.83	1.81
d_8 $[10^{-6}]$	−9.74	−9.71	−9.73	−9.73
d_9 $[10^{-4}]$	3.98	3.96	3.98	3.97
$d_{10}[10^{-1}]$	−6.55	−6.54	−6.55	−6.55

Table 5: Coefficient of the fitting formulae eq. (48) for different final states $f\bar{f}$.

electroweak corrections are still missing, since they involve new topologies with additional top-quark propagators.

Since the numerical effect of the fermionic electroweak two-loop corrections is much larger than the corresponding bosonic contributions, only the fermionic $\mathcal{O}(\alpha^2)$ diagrams are taken into account. As before, the complete one-loop corrections and the (flavor independent) contributions of order $\mathcal{O}(\alpha\alpha_s)$, $\mathcal{O}(\alpha\alpha_s^2)$, $\mathcal{O}(\alpha^2\alpha_s m_t^4)$ and $\mathcal{O}(\alpha^3 m_t^6)$ are also included.

As before, the numerical results are expressed through the parametrization in eq. (48), which reproduces the exact calculation with maximal deviations of 4.5×10^{-6}, when the input parameters stay within their 2σ ranges and the Higgs boson mass in the range 10 GeV $\leq M_H \leq$ 1 TeV. The values of the coefficients for the various final state flavors are listed in Tab. 5.

5.5 Implementation into global Standard Model fits

The fermionic two-loop corrections and some higher-order contributions as listed in eq. (46) are implemented in the current version 6.42 of the program ZFITTER [35,71], which is widely used for global fits of the Standard Model to electroweak precision data [67]. Due to the complexity of the two-loop computation, the implementation of the exact result was not possible, so that instead the numerical fitting formula eq. (48) was included in the code. More details can be found in Ref. [71].

The fitting formula has been incorporated exactly only for the leptonic effective weak mixing angle $\sin^2\theta_{\rm eff}^{\rm lept}$, i.e. for the Zl^+l^- vertex. Results for other light flavors $f = u,d,c,s,\nu$ in the final state are implemented in an approximate way, which reproduces the complete

results of section 5.4 within an error of about 10^{-5} for $f = u, d, c, s$ and 2×10^{-5} for $f = \nu$.

For the $b\bar{b}$ final state, no two-loop electroweak corrections beyond the leading m_{t}^4 are included in ZFITTER 6.42. They shall become available in a future version. However, the current version 6.42 was adjusted with respect to previous version to include complete two-loop corrections in the initial state vertex for the process $e^+e^- \to (Z) \to b\bar{b}$, see Refs. [71,72] for details.

6 Conclusion

In this paper, the evaluation of the complete two-loop contributions to the effective weak mixing angle has been described, expatiating the computational methods and the quantitative implications of the new result.

It was shown how the effective weak mixing angle can be defined at next-to-next-to-leading order through the vector and axial-vector couplings of the Z-boson. The computation of the vertex loop diagrams using two independent techniques for the fermionic part and a combination of several computational methods for the bosonic part was elucidated in detail.

Numerical results for the effective weak mixing angle for different final state flavors were given in terms of accurate numerical parameterizations, which are valid for Higgs masses up to 1 TeV. The new result has been compared in detail with a previous result obtained by an expansion in powers of m_{t} up to next-to-leading order.

Furthermore, the remaining theoretical uncertainties due to unknown higher orders were analyzed and an overall uncertainty of the effective leptonic weak mixing angle $\sin^2\theta_{\mathrm{eff}}^{\mathrm{lept}}$ of 4.7×10^{-5} was estimated.

Electroweak precision data allows very precise tests of the Standard Model at the quantum level and puts the strongest constraints on the Higgs boson mass and new physics. With the completion of the electroweak two-loop corrections, the accuracy of the electroweak precision test was significantly enhanced, with theoretical uncertainties now under much better control.

Acknowledgements

We are grateful to G. Weiglein and K. Mönig for useful discussions and communications. We thank T. Riemann for helping to update the new version of ZFITTER.

The work of M. A. was supported by the BMBF grant No. 05 HT4GUA/4 and by the DFG grant No. SFB 676. The work of M. C. was supported by the Sofja Kovalevskaja Award of the Alexander von Humboldt Foundation sponsored by the German Federal Ministry of Education and Research. A. F. is supported by the Schweizer Nationalfonds.

References

[1] The LEP Collaborations, the LEP Electroweak Working Group and the SLD Electroweak and Heavy Flavour Groups, hep-ex/0412015.

[2] R. Hawkings and K. Mönig, Eur. Phys. J. **directC1**, 8 (1999).

[3] J. Erler, S. Heinemeyer, W. Hollik, G. Weiglein and P. M. Zerwas, Phys. Lett. B **486**, 125 (2000).

[4] A. Freitas, W. Hollik, W. Walter and G. Weiglein, Phys. Lett. B **495**, 338 (2000) [Erratum-ibid. B **570**, 260 (2003)],
M. Awramik and M. Czakon, Phys. Lett. B **568**, 48 (2003).

[5] A. Freitas, W. Hollik, W. Walter and G. Weiglein, Nucl. Phys. B **632**,189 (2002) [Erratum-ibid. B **666**, 305 (2003)].

[6] M. Awramik and M. Czakon, Phys. Rev. Lett. **89**, 241801 (2002);
A. Onishchenko and O. Veretin, Phys. Lett. B **551**, 111 (2003);
M. Awramik, M. Czakon, A. Onishchenko and O. Veretin, Phys. Rev. D **68**, 053004 (2003).

[7] M. Awramik, M. Czakon, A. Freitas and G. Weiglein, Phys. Rev. D **69**, 053006 (2004).

[8] A. Sirlin, Phys. Rev. D **22**, 971 (1980);
W. J. Marciano and A. Sirlin, Phys. Rev. D **22**, 2695 (1980) [Erratum-ibid. D **31**, 213 (1980)].

[9] G. Degrassi and A. Sirlin, Nucl. Phys. B **352**, 342 (1991);
P. Gambino and A. Sirlin, Phys. Rev. D **49**, 1160 (1994).

[10] M. J. Veltman, Nucl. Phys. B **123** 89 (1977).

[11] D. Bardin *et al.*, in *Reports of the Working Group on Precision Calculations for the Z Resonance*, eds. D. Bardin, W. Hollik, G. Passarino, CERN Yellow Report CERN 95-03, p. 7 (1995).

[12] W. Hollik, *Predictions for e^+e^- Processes*, in *Precision Tests of the Standard Model*, ed. P. Langacker (World Scientific, Singapur, 1993), p. 117.

[13] A. Stremplat, Diploma thesis (Univ. of Karlsruhe, 1998).

[14] J. J. van der Bij, K. G. Chetyrkin, M. Faisst, G. Jikia and T. Seidensticker, Phys. Lett. B **498**, 156 (2001);
M. Faisst, J. H. Kühn, T. Seidensticker and O. Veretin, Nucl. Phys. B **665**, 649 (2003).

[15] R. Boughezal, J. B. Tausk and J. J. van der Bij, Nucl. Phys. B **713**, 278 (2005);
R. Boughezal, J. B. Tausk and J. J. van der Bij, Nucl. Phys. B **725**, 3 (2005).

[16] A. Djouadi and C. Verzegnassi, Phys. Lett. B **195**, 265 (1987);
A. Djouadi, Nuovo Cim. A **100**, 357 (1988);
B. A. Kniehl, Nucl. Phys. B **347**, 86 (1990);
F. Halzen and B. A. Kniehl, Nucl. Phys. B **353**, 567 (1991);
B. A. Kniehl and A. Sirlin, Nucl. Phys. B **371**, 141 (1992);
B. A. Kniehl and A. Sirlin, Phys. Rev. D **47**, 883 (1993);
A. Djouadi and P. Gambino, Phys. Rev. D **49**, 3499 (1994) [Erratum-ibid. D **53**, 4111 (1996)].

[17] L. Avdeev, J. Fleischer, S. Mikhailov and O. Tarasov, Phys. Lett. B **336**, 560 (1994) [Erratum-ibid. B **349**, 597 (1994)];
K. G. Chetyrkin, J. H. Kühn and M. Steinhauser, Phys. Lett. B **351**, 331 (1995);
K. G. Chetyrkin, J. H. Kühn and M. Steinhauser, Phys. Rev. Lett. **75**, 3394 (1995).

[18] Y. Schröder and M. Steinhauser, Phys. Lett. B **622**, 124 (2005);
K. G. Chetyrkin, M. Faisst, J. H. Kühn, P. Maierhoefer and C. Sturm, hep-ph/0605201;
R. Boughezal and M. Czakon, hep-ph/0606232.

[19] K. G. Chetyrkin, J. H. Kühn and M. Steinhauser, Nucl. Phys. B **482**, 213 (1996).

[20] J. van der Bij and M. J. Veltman, Nucl. Phys. B **231**, 205 (1984).

[21] J. J. van der Bij and F. Hoogeveen, Nucl. Phys. B **283**, 477 (1987).

[22] R. Barbieri, M. Beccaria, P. Ciafaloni, G. Curci and A. Vicere, Phys. Lett. B **288**, 95 (1992) [Erratum-ibid. B **312**, 511 (1993)];
R. Barbieri, M. Beccaria, P. Ciafaloni, G. Curci and A. Vicere, Nucl. Phys. B **409**, 105 (1993);
J. Fleischer, O. V. Tarasov and F. Jegerlehner, Phys. Lett. B **319**, 249 (1993);
J. Fleischer, O. V. Tarasov and F. Jegerlehner, Phys. Rev. D **51**, 3820 (1995).

[23] G. Degrassi, P. Gambino and A. Sirlin, Phys. Lett. B **394**, 188 (1997).

[24] G. Weiglein, Acta Phys. Polon. B **29**, 2735 (1998).

[25] P. Gambino, A. Sirlin and G. Weiglein, JHEP **9904**, 025 (1999).

[26] M. Awramik, M. Czakon, A. Freitas and G. Weiglein, Phys. Rev. Lett. **93**, 201805 (2004);
M. Awramik, M. Czakon, A. Freitas and G. Weiglein, Nucl. Phys. Proc. Suppl. **135**, 119 (2004);
M. Awramik, M. Czakon, A. Freitas and G. Weiglein, in *Proc. of the International Conference on Linear Colliders (LCWS 04), Paris, France, 19-24 Apr 2004* [hep-ph/0409142].

[27] M. Awramik, M. Czakon and A. Freitas, hep-ph/0605339.

[28] W. Hollik, U. Meier and S. Uccirati, Nucl. Phys. B **731**, 213 (2005).

[29] W. Hollik, U. Meier and S. Uccirati, Phys. Lett. B **632**, 680 (2006).

[30] S. Willenbrock and G. Valencia, Phys. Lett. B **259**, 373 (1991);
A. Sirlin, Phys. Rev. Lett. **67**, 2127 (1991);
R. G. Stuart, Phys. Lett. B **262**, 113 (1991).

[31] H. Veltman, Z. Phys. C **62**, 35 (1994).

[32] M. Passera and A. Sirlin, Phys. Rev. D **58**, 113010 (1998);
P. Gambino and P. A. Grassi, Phys. Rev. D **62**, 076002 (2000);
A. R. Bohm and N. L. Harshman, Nucl. Phys. B **581** 91 (2000).

[33] D. Y. Bardin, A. Leike, T. Riemann and M. Sachwitz, Phys. Lett. B **206**, 539 (1988).

[34] U. Baur *et al.*, hep-ph/0202001, in *Proc. of the APS/DPF/DPB Summer Study on the Future of Particle Physics (Snowmass 2001)* eds. R. Davidson and C. Quigg.

[35] D. Y. Bardin, P. Christova, M. Jack, L. Kalinovskaya, A. Olchevski, S. Riemann and T. Riemann, Comput. Phys. Commun. **133**, 229 (2001).

[36] M. Böhm and W. Hollik, Nucl. Phys. B **204**, 45 (1982).;
S. Jadach, J. H. Kühn, R. G. Stuart and Z. Wąs, Z. Phys. C **38**, 609 (1988) [Erratum-ibid. C **45**, 528 (1990)].

[37] F. A. Berends, W. L. van Neerven and G. J. H. Burgers, Nucl. Phys. B **297**, 429 (1988) [Erratum-ibid. B **304**, 921 (1988)];
F. A. Berends *et al*, in *Z Physics at LEP 1*, eds. G. Altarelli, R. Kleiss and C. Verzegnassi (CERN-89-08), p. 89;
M. Skrzypek and S. Jadach, Z. Phys. C **49**, 577 (1991);
M. Skrzypek, Acta Phys. Polon. B **23**, 135 (1992);
M. Cacciari, A. Deandrea, G. Montagna and O. Nicrosini, Europhys. Lett. **17**, 123 (1992).

[38] M. Greco, G. Pancheri-Srivastava and Y. Srivastava, Nucl. Phys. B **171**, 118 (1980) [Erratum-ibid. B **197**, 543 (1982)];
F. A. Berends, R. Kleiss and S. Jadach, Nucl. Phys. B **202**, 63 (1982).

[39] A. B. Arbuzov, D. Y. Bardin and A. Leike, Mod. Phys. Lett. A **7**, 2029 (1992) [Erratum-ibid. A **9**, 1515 (1994)].

[40] S. Jadach, B. F. L. Ward and Z. Wąs, Comput. Phys. Commun. **79**, 503 (1994).

[41] M. L. Nekrasov, talk presented at the XVth International Workshop *High Energy Physics and Quantum Field Theory*, Tver, September 2000, hep-ph/0102284;
B. A. Kniehl and A. Sirlin, Phys. Lett. B **530**, 129 (2002).

[42] A. I. Davydychev and J. B. Tausk, Nucl. Phys. B **397**, 123 (1993).

[43] S. Bauberger, F. A. Berends, M. Böhm and M. Buza, Nucl. Phys. B **434**, 383 (1995).

[44] S. Bauberger and M. Böhm, Nucl. Phys. B **445**, 25 (1995).

[45] G. Degrassi, P. Gambino and A. Vicini, Phys. Lett. B **383**, 219 (1996).

[46] B. A. Kniehl and J. H. Kühn, Nucl. Phys. B **329**, 547 (1990).

[47] A. V. Kotikov, Phys. Lett. B **259**, 314 (1991);
E. Remiddi, Nuovo Cim. A **110**, 1435 (1997).

[48] K. G. Chetyrkin and F. V. Tkachov, Nucl. Phys. B **192**, 159 (1981).

[49] R. J. Gonsalves, Phys. Rev. D **28**, 1542 (1983);
G. Kramer and B. Lampe, J. Math. Phys. **28**, 945 (1987).

[50] N. Nielsen, Nova Acta Leopoldina (Halle) 90, 123 (1909).

[51] L. Lewin, *Polylogarithms and Associated Functions*, North Holland (1981).

[52] B. Feucht, J. H. Kühn and S. Moch, Phys. Lett. B **561**, 111 (2003).

[53] U. Aglietti and R. Bonciani, Nucl. Phys. B **668**, 3 (2003);
U. Aglietti and R. Bonciani, Nucl. Phys. B **698**, 277 (2004).

[54] S. Laporta, Int. J. Mod. Phys. A **15**, 5087 (2000).

[55] T. Gehrmann and E. Remiddi, Nucl. Phys. B **580**, 485 (2000).

[56] M. Czakon, DiaGen/IdSolver (*unpublished*);
see also M. Awramik, M. Czakon, A. Freitas and G. Weiglein, Nucl. Phys. Proc. Suppl. **135**, 119 (2004).

[57] A. Czarnecki, U. Kilian and D. Kreimer, Nucl. Phys. B **433**, 259 (1995);
A. Frink, B. A. Kniehl, D. Kreimer and K. Riesselmann, Phys. Rev. D **54**, 4548 (1996);
A. Frink, U. Kilian and D. Kreimer, Nucl. Phys. B **488**, 426 (1997).

[58] A. Ghinculov and J. J. van der Bij, Nucl. Phys. B **436**, 30 (1995).

[59] M. Czakon, hep-ph/0511200.

[60] V. A. Smirnov, Phys. Lett. B **460**, 397 (1999);
J. B. Tausk, Phys. Lett. B **469**, 225 (1999).

[61] C. Anastasiou and A. Daleo, hep-ph/0511176.

[62] V. A. Smirnov, *"Applied asymptotic expansions in momenta and masses"*, Springer, Berlin, Germany (2002).

[63] A. V. Kotikov, Phys. Lett. B **254**, 158 (1991);
A. V. Kotikov, Phys. Lett. B **259**, 314 (1991).

[64] E. Remiddi, Nuovo Cim. A **110**, 1435 (1997).

[65] T. Binoth and G. Heinrich, Nucl. Phys. B **585**, 741 (2000);
T. Binoth and G. Heinrich, Nucl. Phys. B **680**, 375 (2004).

[66] M. Czakon, M. Awramik and A. Freitas, in *Proc. of 7th International Symposium on Radiative Corrections (RADCOR 2005), Shonan Village, Kanagawa, Japan, 2-7 Oct 2005* [hep-ph/0602029].

[67] `http://lepewwg.web.cern.ch/LEPEWWG/`.

[68] S. Eidelman *et al.* [Particle Data Group Collaboration], Phys. Lett. B **592**, 1 (2004); also 2005 partial update for edition 2006, available on `http://pdg.lbl.gov`.

[69] D. Y. Bardin, A. Leike, T. Riemann and M. Sachwitz, Phys. Lett. B **206**, 539 (1988).

[70] G. Degrassi, P. Gambino, M. Passera and A. Sirlin, Phys. Lett. B **418**, 209 (1998).

[71] A. B. Arbuzov, M. Awramik, M. Czakon, A. Freitas, M. W. Grünewald, K. Mönig, S. Riemann, T. Riemann, Comput. Phys. Commun. **174**, 728 (2006).

[72] A. Freitas and K. Mönig, Eur. Phys. J. C **40**, 493 (2005).